Axonal degeneration induced by glutamate-excitotoxicity is mediated by necroptosis.

Diego E. Hernández[1, 2, 3], Natalia A. Salvadores[1, 4], Guillermo Moya-Alvarado[5], Romina J. Catalán[1, 4], Francisca C. Bronfman[5] and Felipe A. Court [1, 4, 6 #]

[1]Center for Integrative Biology, Faculty of Sciences, Universidad Mayor, Chile. [2]Cold Spring Harbor Laboratory, Cold Spring Harbor, NY 11724, USA. [3]Center of Advanced Microscopy (CMA), Universidad de Concepción, Concepción, Chile. [4]FONDAP Center for Geroscience, Brain Health and Metabolism, Santiago, Chile. [5]Center for Ageing and Regeneration (CARE UC), Faculty of Biological Sciences, Department of Physiology, Pontificia Universidad Católica de Chile, Santiago, Chile. [6]Buck Institute for Research on Ageing, Novato, San Francisco, USA.

[#]**Corresponding author:** Felipe A. Court, Center for Integrative Biology, Faculty of Sciences, Universidad Mayor, Chile. E-mail: felipe.court@umayor.cl

Keywords: Neurodegeneration, axonal degeneration, excitotoxicity, necroptosis

Summary statement:

The role of necroptotic signaling at the control of the axonal degeneration mechanism during neuronal excitotoxic damage.

Abstract

Neuronal excitotoxicity induced by glutamate leads to cell death and functional impairment in a variety of central nervous system pathologies. Glutamate-mediated excitotoxicity triggers neuronal apoptosis in the cell soma as well as degeneration of axons and dendrites by a process associated to calcium increase and mitochondrial dysfunction. Importantly, degeneration of axons initiated by diverse stimuli, including excitotoxicity, has been proposed as an important pathological event leading to functional impairment in neurodegenerative conditions. Here we demonstrate that excitotoxicity-induced axonal degeneration proceeds by a mechanism dependent on the necroptotic kinases RIPK1, RIPK3 and the necroptotic mediator MLKL. Inhibition of RIPK1, RIPK3 or MLKL prevent key steps in the axonal degeneration cascade including mitochondrial depolarization, the opening of the permeability transition pore and calcium dysregulation in the axon. Interestingly, the same excitotoxic stimuli lead to apoptosis in the cell soma, demonstrating the co-activation of two independent degenerative mechanisms in different compartments of the same cell. The identification of necroptosis as a key mechanism of axonal degeneration after excitotoxicity is an important initial step to develop novel therapeutic strategies for nervous system disorders.

JCS Advance Online Article. Posted on 17 October 2018

Introduction

Neuronal excitotoxicity has been described as a contributing factor in several pathologies of the central nervous system (CNS), including Alzheimer´s disease (AD), Huntington's disease (HD), Amyotrophic Lateral Sclerosis (ALS), Parkinson´s disease (PD), epilepsy, cerebrovascular accidents, ischemia, hypoxia and mechanical trauma (Mehta et al., 2013). Excitotoxicity take place as a result of excessive release of the neurotransmitter glutamate, which in turn activates a variety of synaptic and extra-synaptic glutamate receptors in neurons, leading to calcium overload and neuronal death (Castilho et al., 1998; Lau and Tymianski, 2010).

As glutamate receptors are expressed in the neuronal soma, dendrites, axons and terminals(Hosie et al., 2012; Lau and Tymianski, 2010; Stirling and Stys, 2010), glutamate excitotoxicity is found in different neuronal compartments. Indeed, it has been demonstrated that glutamate excitotoxicity leads to neuronal apoptosis (Ankarcrona et al., 1995), as well as degeneration of axons and dendrites (Hosie et al., 2012). Importantly, axonal degeneration is a common feature of neurodegenerative conditions exhibiting excitotoxicity (Salvadores et al., 2017), including ALS (Fischer et al., 2004), AD (Adalbert et al., 2009), PD (Tagliaferro and Burke, 2016) and poly-glutamine disorders (Diprospero et al., 2004), representing a target for neuroprotection (Coleman and Perry, 2002). Studies in the Wld^S mutant mice and *Sarm1*-null mice, in which axonal degeneration is strongly delayed, demonstrated the existence of a regulated mechanism for axonal degeneration (Conforti et al., 2014). Moreover, expression of the Wld^S gene or loss of function of Sarm1 in models of neuropathies and neurodegenerative diseases have been shown to delay in some situations pathological events and functional deficits (Conforti et al., 2014).

Axonal degeneration -a non-apoptotic programed cell death mechanism- is characterized by an increase in axonal free calcium (Ca^{2+}) released from the endoplasmic reticulum (Villegas et al., 2014), which triggers the opening of the mitochondrial permeability transition pore (mPTP) (Barrientos et al., 2011), leading to a decrease in mitochondrial membrane potential, increase in reactive oxygen species (ROS) (Calixto et al., 2012), energetic failure (Villegas et al., 2014), and activation of proteases that degrade the axon, including calpains and caspases (Ma et al., 2013). Even though several steps in the axonal degenerative program have been described, a common upstream signaling pathway activated by diverse stimuli leading to degeneration has not yet been identified. Interestingly, some events in the axonal degeneration cascade, including mitochondrial dysfunction, ROS production and membrane permeabilization are commonly associated to necroptosis, a regulated form of necrotic cell death (Vandenabeele et al., 2010b).

Necroptosis was first described in the context of TNFα receptor 1 (TNFR1) activation by TNFα, a death ligand that induces necroptosis upon formation of a protein complex known as the necrosome (Vandenabeele et al., 2010b). Necrosome formation leads to cell dismiss with cellular and organelle swelling, mitochondrial dysfunction, chromatin condensation and plasma membrane permeabilization (Vandenabeele et al., 2010b). It was later demonstrated that necroptosis can be initiated by a wide variety of stimuli, including TNFα, lipopolysaccharide, endoplasmic reticulum stress, viral infection and increase in intracellular calcium (Kaczmarek et al., 2013). The canonical necroptotic response depends

on the state of ubiquitylation of receptor interacting kinase 1 (RIPK1) (Brenner et al., 2015). Deubiquitylation of RIPK1 mediated by the absence of RIPK1-ubiquitylases including cellular inhibitor of apoptosis 1 or 2 (cIAP 1 and cIAP 2), or by the activation of cylindromatosis deubiquitylase (CYLD), promote the association of RIPK1 with cytosolic protein complexes known as Complex IIa, IIb or the necrosome, inducing apoptosis or necroptosis depending on caspase-8 activity (Brenner et al., 2015). Complex IIa and Complex IIb promote apoptosis through the activation of a caspase-8 dependent cascade, and the processing and inhibition of RIPK1 and RIPK3. In turn, necroptosis is induced by the formation of the necrosome complex, constituted by caspase-8, RIPK1, receptor-interacting kinase 3 (RIPK3), FAS-associated death domain (FADD), and the short ($FLIP_S$) or long ($FLIP_L$) isoforms of the FLICE-like inhibitory protein (Brenner et al., 2015). Necrosome activation takes place under pharmacological, viral or endogenous ($FLIP_S$) caspase-8 inhibition, triggering RIPK1 auto-phosphorylation, RIPK3 phosphorylation by phosphorylated RIPK1 (pRIPK1) and MLKL phosphorylation by pRIPK3. Translocation of pMLKL to the plasma membrane, leads to the formation of the 'MLKL channel' that increase Na^+ influx and subsequent osmotic stress (Chen et al., 2014).

Importantly, necroptosis has been shown to be involved in neuronal dysfunction in models of pathologies with prominent axonal degeneration in which glutamate excitotoxicity is also a contributing factor. Examples include MS (Ofengeim et al., 2015), ALS (Ito et al., 2016), AD (Caccamo et al., 2017), ischemic brain damage (Chavez-Valdez et al., 2012; Chen et al., 2018), cortical trauma (You et al., 2008), spinal cord injury (Wang et al., 2015) and retinal damage (Dong et al., 2012; Rosenbaum et al., 2010). Although these data demonstrate the functional involvement of necroptotic cell death in complex CNS disorders, whether necroptosis directly participates in axonal and dendrite degeneration after excitotoxicity remains unknown.

Here we demonstrate that excitotoxicity-induced axonal degeneration proceeds by a necroptotic mechanism, which activate mitochondrial mPTP, and calcium dysregulation in the axonal compartment without the requirement of caspase inhibition. Surprisingly, neuronal soma degenerates simultaneously by canonical apoptosis, demonstrating differential death mechanisms in two cellular compartments under the same pro-degenerative stimulus. As axonal degeneration has been associated to several neurodegenerative conditions in their early phases, the participation of necroptotic-associated pathways unravel novel regulators of the axonal degenerative cascade, an important step to develop therapeutic strategies for nervous system disorders.

Results

RIPK1 inhibitors prevent glutamate-dependent RIPK1 phosphorylation and delays neurite degeneration in hippocampal neurons.

The involvement of RIPK1 in neurite degeneration induced by glutamate excitotoxicity was evaluated in rat embryonic hippocampal neurons using nec-1, a well characterized RIPK1 inhibitor, and nec-1s which presents a higher specificity for RIPK1 (Takahashi et al., 2012). Cultures of hippocampal neurons

were exposed to glutamate (20 µM for 6 hours) or vehicle as a control, in the presence or absence of nec-1 or nec-1s (100 µM). After treatment, hippocampal neurons were immunostained with antibodies for acetylated tubulin (Ac-Tub) and neurofilament medium polypeptide (NF-M) to evaluate neuronal morphology and cytoskeleton integrity, respectively and counterstained with DAPI to characterize nuclear morphology (**Fig. 1A**). After 6 hours, glutamate treatment induced the fragmentation of the cytoskeleton and neurite beading. In addition, glutamate treatment increased the percentage of neuronal soma with condensed nuclei (pyknosis) compared to control conditions (**Figs. 1A**, **S1A,B**). Quantitative assessment of degeneration using the neurite integrity index (See **Fig. S2A,** and method section) shown that the treatment of hippocampal neurons with glutamate in the presence of nec-1 (or nec-1s) strongly delayed neurite degeneration compared to glutamate alone after 6 and even 24 hours of treatment (**Figs. 1A,B, S2A, S3**). Nevertheless, glutamate-induced nuclei condensation was not prevented by nec-1 or nec-1s (**Figs. 1A, S1A,B**). Importantly, nec-1 and nec-1s alone did not alter neurite and nuclear morphology of hippocampal neurons (**Figs. 1A,B**, **S1A,B**).

The phosphorylation of RIPK1, has been functionally associated to RIPK1 activation (Vandenabeele et al., 2010a). To study if the observed protective effect of RIPK1 inhibition over neurite degeneration is related to changes in RIPK1 phosphorylation, the relative levels of phosphorylated RIPK1 (pRIPK1) were evaluated by western blot, using protein samples from 7-8DIV cultured hippocampal neurons exposed to glutamate (20 µM glutamate for 1,5 hours) or vehicle as a control, in the presence or absence of nec-1 (100 µM). Phosphorylated RIPK1 was resolved from unphosphorylated RIPK1, by poly-acrylamide gel electrophoresis in the presence of Phostag™ additive (see methods). Compared to control conditions, glutamate induced a significant increase in the relative levels of pRIPK1 compared to the total levels of RIPK1 (**Fig. 1C**) and nec-1 prevented the glutamate-induced changes in the relative amount of pRIPK1 (**Fig. 1C**). As expected by the glutamate induced neuronal degeneration, lower levels of protein were observed for RIPK1 and Hsp90, the last used as a protein loading control (**Fig. S2B**). Nevertheless, the relative amount of total RIPK1 remained unaffected by treatments with glutamate or nec-1 compared to untreated neuronal cultures after normalization by Hsp90 protein levels (**Fig. S2B**).

In equivalent conditions, the treatment with glutamate (20 µM glutamate for 1,5 hours) induce an increase in the relative levels of phospho-RIPK3 (antibody designed against murine phopho-S232-RIPK3; pRIPK3) (Chen et al., 2013) compared with the vehicle condition in the neuronal culture protein samples (**Fig. 2A**). In equivalent neuronal culture lysates, pMLKL co-immunoprecipitation using RIPK1 as immunoprecipitation ligand was done to evaluate the formation of the necrosome complex after the glutamate stimuli. Glutamate treatment induced an increase in the relative amount of co-immunoprecipitated phospho-MLKL (antibody designed against murine phospho-S345-MLKL; pMLKL) (Rodriguez et al., 2015) compared to the vehicle condition (**Fig. 2B**), suggesting the formation of the necrosome complex after the excitotoxic stimuli. IgG western-blot was done as loading control (**Fig. 1E**). Western blot against the IgG was used as a loading control of the immunoprecipitated samples (**Fig. 2B**).

To directly assess the effect of glutamate and RIPK1 inhibition over the activation of necroptotic factors in the axonal compartment, 7-8DIV cultured hippocampal neurons were exposed to glutamate (20 µM

for 3 hours) with or without nec-1s pre-treatment and subjected to immunofluorescence staining using an antibody against pMLKL and TAU1 as an axonal-specific marker (**Fig. 1D**). Significantly higher relative levels of pMLKL were observed in axons form neurons exposed to glutamate compared to the vehicle control condition. The observed increase in axonal pMLKL induced by glutamate was prevented by nec-1s pre-treatment (**Figs. 1D, 2C**). To control the effects of glutamate treatment and RIPK1 inhibition over TAU1 axonal stain, cultured hippocampal neurons with 7-8DIV were exposed to glutamate (20 µM for 3 hours) with or without nec-1s pre-treatment and immunostained against TAU1 and MAP2 to identify the somato-dendritic compartment. In vehicle control conditions, a continuous pattern of TAU1 staining with sporadic TAU1-positive puncta was obtained (**Fig. S1E,F**). Glutamate treatment induced an increase in the mean number of puncta in TAU1-positive axons (**Fig. S1E,F**), changes associated to beading formation during the progression of axonal degeneration. Importantly, RIPK1 inhibition using nec-1s prevented beading formation induced by glutamate (**Fig. S1E,F**).

Together this data shown that RIPK1 inhibition prevents glutamate induced neurite degeneration. In addition, glutamate treatment induces an early RIPK1, RIPK3 and MLKL phosphorylation, together with an increase in pMLKL co-immunoprecipitation with RIPK1, suggesting the formation of the necrosome complex.

RIPK3 and MLKL knock-down delay neurite degeneration in hippocampal neurons exposed to glutamate.

RIPK3 and MLKL knock-down using shRNA were used to evaluate the participation of RIPK3 and MLKL in glutamate-induced neurite degeneration. Cultured hippocampal neurons were electroporated with a mix of plasmids containing shRNA sequences designed to knock-down RIPK3 or infected with lentivirus expressing shRNA to knock-down MLKL expression. The used shRNA constructs co-express GFP as a reporter gene to identify electroporated or infected neurons and for subsequent neurite morphology analysis.

Neurons electroporated with either RIPK3 or scramble shRNA plasmids were exposed to vehicle or glutamate (20 µM) for 6 hours. To control RIPK3 knock-down in electroporated neurons, protein samples from cultures of hippocampal neurons were collected and used for western-blot of RIPK3 and Hsp90 as a loading control (**Fig. 3A, left**). Densitometry analysis show that RIPK3 shRNA electroporated neurons expressed significantly less RIPK3 compared to neurons electroporated with the scramble shRNA construct (**Fig. 3A, right**). Neurons were fixed and immuno-stained against Ac-Tub and GFP, together with DAPI for nuclear staining (**Fig. 3B**). For quantification of neurite degeneration, neurites of electroporated neurons were classified as continuous, beaded or fragmented and represented as a percentage of the total analyzed neurites (**Fig. 3C**). A continuous morphology is associated with a healthy neurite and both beaded and fragmented morphologies represent progressive stages of degeneration. For neurons electroporated with a scramble shRNA, glutamate treatment induced a significant increase in the percentage of fragmented neurites and a significant decrease in continuous neurites (**Fig. 3B,D**). In contrast, neurons electroporated with the RIPK3 shRNA construct were strongly protected from glutamate-induced neurite beading and fragmentation (**Fig. 3B,D**). In

addition, glutamate treatment in both scramble and RIPK3 shRNA electroporated neurons induced a significant increase in the number of nuclei showing condensed morphology when compared to vehicle treated neurons, with a slightly but significant reduction of condensed nuclei in neurons electroporated with RIPK3 shRNA compared to the scramble electroporated control (**Fig. S1C**).

Similar results regarding neurite degeneration were achieved by MLKL knock-down. Cultured hippocampal neurons were infected with lentiviruses expressing shRNA against MLKL or scramble sequences. Glutamate treatment (20 µM for 6 hours) induced a significant increase in the percentage of neurites showing beaded or fragmented morphology compared with the scramble and shRNA-MLKL vehicle controls (**Figs. 3E, S4**). The knock-down of MLKL strongly from glutamate-induced neurite beading and fragmentation (**Figs. 3E, S4**).

RIPK1 inhibition does not prevent glutamate-induced apoptotic cell death of hippocampal somas.

As described before in **Figs. 1A, 3B and S1,A,B,C,** RIPK1 inhibition, and RIPK3 knock-down do not prevent neuronal death induced by glutamate excitotoxicity. To evaluate which kind of cell death was induced by glutamate treatment in neuronal somas where necroptotic neurite degeneration was observed, TUNEL and PI exclusion assays were used to identify apoptotic and necrotic cell death, respectively. Together with these assays, electron microscopy (EM) was also performed in equivalent treatments to ultra-structurally discriminate between each type of cell death. Cultured hippocampal neurons were treated with glutamate (20 µM for 6 hours) with or without nec-1 treatment (100 µM). Compared to control conditions, glutamate treatment induced a significant increase in the percentage of TUNEL-positive neuronal nuclei. Moreover, glutamate treatment did not induce significant increase in the percentage of PI-positive nuclei (**Figs. 4A**,**B,C**). Ultra-structurally, glutamate induced nuclei condensation in neuronal somas without extensive membrane breakdown or organelle swelling (**Fig. 4A**). Nec-1 treatment did not prevent the increase in the percentage of TUNEL-positive nuclei and the ultrastructural changes induced by glutamate (**Fig. 4A,B**), suggesting that degenerative mechanisms activated by glutamate in the neuronal soma correspond to an apoptotic cascade independent from RIPK1. Treatment with H_2O_2 (50 µM for 4 hours) was included as a positive control for the PI exclusion assay, that shown a significant increase in PI-positive nuclei compared to control conditions (**Figs. 4A**,**C, S1D**).

Axonal degeneration is prevented by RIPK1 inhibition in the axonal compartment in glutamate treated neurons.

Pharmacological inhibition of RIPK1 or genetic knock-down of RIPK3 inhibits neurite degeneration but not nuclear apoptosis after glutamate excitotoxicity, suggesting the activation of different cell death mechanisms in the soma versus the axon compartment. To test if the protective effect of targeting RIPK1 was specific to the axonal compartment, hippocampal neurons were growth in microfluidic devices to spatially isolate axons from neuronal somas. Neurons were seeded in one of the compartments of each microfluidic device and extending axons reached the second compartment by

crossing micro grooves small enough to restrain somas from crossing at the step of neuronal seeding. The maintenance of a higher volume of media in the neuronal compartment of the microfluidic device, allowed axonal specific treatment by the presence of positive hydrostatic pressure towards the axonal compartment **(Fig. 5A)**. Neurons were exposed to glutamate treatment (20 µM) for 6 hours in the neuronal compartment of the microfluidic device and only axons were treated with nec-1 (100 µM) or vehicle solution in the axonal compartment of the microfluidic device. In these conditions, glutamate treatment induced an increase in axonal fragmentation revealed by both Ac-Tub and NF-M staining (**Fig. 5B**), and a significant decrease in the axonal integrity index (**Fig. 5C**). Treatment of axons with nec-1 prevented the fragmentation induced by glutamate treatment (**Fig. 5B,C**). Importantly, nec-1 treatment in the absence of glutamate did not produce noticeable effects in neurite morphology compared to control conditions (**Fig. 5B,C**). Together, these results suggest that axonal degeneration induced by neuronal excitotoxicity can be prevented by inhibiting RIPK1 in the axonal compartment.

Glutamate-induced mitochondrial dysfunction in neurites is prevented by RIPK1 inhibition.

Axonal degeneration after mechanical damage is associated to mitochondrial dysfunction, including a decline in mitochondrial membrane potential and opening of the mPTP (Barrientos et al., 2011). In these injured axons, mitochondrial responses are associated to a rise in the cytoplasmic free-Ca^{2+} levels, which is also a well-known effect of glutamate-induced excitotoxicity. Therefore, we evaluated whether inhibition of necroptotic factors prevents neurite and/or axonal mitochondrial dysfunction induced by excitotoxicity. We assessed mitochondrial function using the potential-sensitive probe TMRM and evaluated the opening of the mPTP by the calcein-cobalt staining method in live-cells exposed to glutamate with or without nec-1 treatment. Compared to control conditions, glutamate (20 µM) treatment for 1,5 hours induced a decrease in TMRM mean fluorescence of individual mitochondrion located in neurites of dissociated hippocampal neuronal cultures and in axonal mitochondria of compartmentalized hippocampal neuron cultures (**Fig. 6**). Nec-1 pre-treatment prevented the change in the frequency distribution of TMRM fluorescence of neurite mitochondrion induced by glutamate treatment (**Fig. S5A)**, and the decrease in the mean TMRM fluorescence induced by glutamate (**Fig. 6A,B**). In a similar way, the shRNA mediated knock-down of RIPK3 or MLKL using lentiviruses prevented the decrease in the TMRM fluorescence induced by glutamate treatment in neurite mitochondria from GFP positive infected neurons (**Fig. 6C, D)**. In compartmentalized cultures (**Fig. 5A**), nec-1s treatment in the axonal compartment significantly prevented the decrease in mean axonal mitochondrial TMRM fluorescence induced by glutamate treatment at the neuronal soma (**Fig. 6E,F**).

The calcein-cobalt staining method was used to evaluate glutamate effects over mPTP opening at neurite mitochondria. This method relays in the loss of calcein staining in mitochondria after mPTP opening (see methods). Compared to control conditions, neurite mitochondrion exposed to glutamate exhibited a significant loss of co-localization between mitotracker- stained mitochondria and calcein staining (**Fig. 7A,B**). The treatment with nec-1 prevented the glutamate-dependent decrease in co-localization between mitotracker and calcein (**Fig. 7A,B**). Other mitochondrial parameters associated with mPTP activation are mitochondrial fission and increase in circularity by mitochondrial swelling. Consistently, neurite mitochondrial shown a decrease in their length and an increase in their circularity

after the glutamate treatment (**Fig. 7C,D**). Nec-1 pre-treatment prevented morphological parameter changes induced by glutamate treatment (**Fig. 7C,D**). Importantly, nec-1 treatment without glutamate did not affect the percentage of mitochondria showing mPTP opening or changed mitochondrial length and/or circularity (**Fig. 7**).

RIPK1 inhibition prevents axonal calcium dys-homeostasis in cultured hippocampal neurons after glutamate treatment.

The rise in free-Ca^{2+} cytoplasmic levels is a well-known effect of excitotoxicity induced by glutamate and other pro-degenerative stimuli in axons, including mechanical damage and chemotherapy induced axonal degeneration (Avery et al., 2012; Villegas et al., 2014). Therefore, we evaluated the effects of RIPK1 inhibition over glutamate-dependent changes in calcium dynamics in somas and neurites of hippocampal neurons. Neurons were loaded with the calcium-sensitive indicator Fura-2 and the effect of glutamate treatment in the presence or absence of nec-1 was registered by time-lapse microscopy. In both neurites and soma, glutamate (20 µM) induced an immediate rise in the levels of cytoplasmic free-Ca^{2+} (**Figs. 8A,B**, **S6A,B**). In glutamate-treated neurites, the initial rise in cytoplasmic free-Ca^{2+} levels were maintained in a steady state for approximately 30 minutes followed by a second phase of calcium rise, known as delayed calcium dys-homeostasis (DCD) that can be analyzed by measuring the slope between the thirty and 90 minutes of recording (**Fig. 8C**). In nec-1 treated hippocampal neurons, glutamate induced a first rise of cytoplasmic free-Ca^{2+} in neurites comparable to the changes recorded in neurites from cultures treated with glutamate only (**Fig. 8A,B**). Nevertheless, nec-1 treatment significantly prevented the glutamate-induced DCD (**Fig. 8A,B,C**). As it has been described that the mPTP opening is the point of no-return in axonal degeneration (Barrientos et al., 2011), experiments with the mPTP blocker CsA were performed to understand the effects of mPTP opening in neurite calcium dys-homeostasis. In neurites, the treatment with CsA (50 µM) prevented the DCD induced by glutamate treatment, and the effect is comparable to nec-1 treatment in the same excitotoxic conditions (**Fig. 8A,B,C**). Importantly, treatments with, vehicle, nec-1 or CsA alone did not have noticeable effect over the levels of cytoplasmic free-Ca^{2+} along the whole recording time (**Fig. 8A,B**). Similar experiments were performed in compartmentalized cultures to show the specific effect of RIPK1 inhibition over axonal calcium dys-homeostasis (**Fig. 5A**). Axoplasmic free-Ca^{2+} levels at zero, thirty, sixty and ninety minutes were recorded using snap-shots of fields with axons charged with the non-ratiometric calcium probe fluo4. Glutamate treatment (20 µM) in the neuronal compartment of the microfluidic device, induced a progressive and significant increase in the axoplasmic free-Ca^{2+} levels that is evident after ninety minutes of glutamate treatment (**Figs. 8D,E, S6C**). Inhibition of RIPK-1 with nec-1s prevented the glutamate-induced increase of axoplasmic free-Ca^{2+} levels at ninety minutes compared with the zero, thirty- and sixty-minutes snap-shots. Vehicle and nec-1s controls had no significant difference in the axoplasmic free-Ca^{2+} levels at the different snap-shot times (**Figs. 8E, S6C)**.

In somas, glutamate induced a fast rise in cytoplasmic free-Ca^{2+} levels that decayed with time, and that never reached basal cytoplasmic free-Ca^{2+} levels during the recording time **(Fig. S6A,B)**. Nec-1 treatment only had a transient effect over the glutamate induced neuronal soma free-Ca^{2+} dynamics, that shown a decrease in the amplitude of the cytoplasmic free-Ca^{2+} rise in the first minutes after

glutamate treatment but was followed by levels of cytoplasmic free-Ca^{2+} comparable to the glutamate alone treatment during the recorded time **(Fig. S6A,B)**. Vehicle and nec-1 control treatments shown steady basal levels of cytoplasmic free-Ca^{2+} during the recorded time **(Fig. S7B)**.

Discussion

Neuronal degeneration triggered by excitotoxicity leads to the loss of nervous system function in a variety of neurodegenerative conditions. Nevertheless, beyond neuronal cell death, the mechanism by which excitotoxicity leads to degeneration of axons remained unknown. Degeneration of neuronal extensions has been intensively studied as a critical degenerative process during early stages of neurodegeneration. The identification of several proteins that modify the course of axonal degeneration, including Wld^{s}, CypD, dSARM and Axed (Barrientos et al., 2011; Coleman and Freeman, 2010; Neukomm et al., 2017; Osterloh et al., 2012), and their conserved function in distant organisms, including worms (Calixto et al., 2012), flies (Avery et al., 2012) and vertebrates (Vargas et al., 2015), suggests an evolutionary conserved and therefore crucial function for axonal degeneration in adult organisms. Our results suggest that glutamate-induced axonal degeneration proceed by necroptosis, through the activation of RIPK1,RIPK3 and MLKL, and executed by a calcium and mPTP-dependent mechanism, which has been previously implicated in Wallerian degeneration (Barrientos et al., 2011; Villegas et al., 2014).

Inhibition of RIPK1 and knock-down of RIPK3 and MLKL in cultured hippocampal neurons, delayed glutamate-induced neurite degeneration without inhibiting apoptosis of neuronal somas. These results are consistent with studies in other models of neuronal degeneration showing that soma and neurite degeneration are controlled by different degenerative mechanisms (Ikegami and Koike, 2003).

Necroptosis, through the activation of RIPK1 and RIPK3, has been shown to mediate loss of nervous system function in several pathologies, including those associated to secondary excitotoxic damage (Chavez-Valdez et al., 2012; Liu et al., 2014a). Loss of axons and dendrites correspond to early and common features of most of these animal models of neurodegenerative conditions (Lingor et al., 2012), therefore a common mechanism associated to neuronal dysfunction in these pathologies might correspond to necroptotic-dependent axonal degeneration. Furthermore, some experimental evidences suggest that neuronal apoptosis could be secondary to axonal loss (Ikegami and Koike, 2003).

Several studies *in vitro* have demonstrated that necroptosis become activated only after caspase inhibition, as caspase-8 is part of the death complex II, acting as a negative regulator of necroptosis by cleaving RIPK1 (Vandenabeele et al., 2010b). However, in neurons caspase-8 inhibition is not necessary for the engagement of necroptosis resulting in neuronal cell death (Li et al., 2008). Consistently, our results demonstrate that glutamate-induced RIPK1, RIPK3 and MLKL activation in neurites occur in conditions in which caspases have not been inhibited by experimental interventions, suggesting the lack of caspase-8 activity or their expression in neurites allows necroptosis to proceed after glutamate-mediated excitotoxicity. Moreover, caspase-8 expression is downregulated after OGD

or ischemia (Vieira et al., 2014; Xu et al., 2016), raising another mechanistic explanation for caspase-independent activation of necroptosis in neurites.

In non-neuronal cells, several stimuli act as necroptotic inductors through the activation of different signaling transductors, including TNFR-1, TNFR-2, CD95R, TRAILR-1, TRAILR-2, PAMPs receptors, DAMPs receptors and increase in cytoplasmic free-calcium (Kaczmarek et al., 2013). In the context of our studies, a raise in cytoplasmic calcium after glutamate treatment corresponds to the most plausible explanation for necroptosis activation. In human SK-N-SH neuroblastoma cells, HVJ-E sendai virus infection induces RIPK1 phosphorylation and necroptosis cell death by a CaMKII dependent mechanisms (Nomura et al., 2014). CaMKII is a broadly expressed kinase in CNS neurons and a major regulator of neuronal calcium signaling (Wayman et al., 2008), as well as glutamatergic excitotoxicity responses (Ashpole and Hudmon, 2011). Therefore, cytoplasmic calcium overload during excitotoxic stimuli might lead to necroptosis by phosphorylation of RIPK1 after calcium-dependent CaMKII activation. De-ubiquitylation of RIPK1 by CYLD leads to necroptosis by activating necrosome formation (Brenner et al., 2015) and CaMKII-dependent CYLD activation after NMDA excitotoxicity has been described in hippocampal neurons (Thein et al., 2014). Therefore, axonal activation of CaMKII by an increase in cytoplasmic calcium after glutamatergic excitotoxicity, might directly activate RIPK1 or/and indirectly through CYLD.

Interestingly, it has been shown that activation of RIPK1 and RIPK3 trigger similar processes during necroptosis in different cell types (Kaczmarek et al., 2013). For instance, in tumoral cells, phosphorylation of RIPK3 activates calpains and induce membrane damage by phospholipase A2-mediated production of arachidonic acid and lipid hydro-peroxidation (Shang et al., 2014; Sosna et al., 2014). Both calpain activation and phospholipase A2-mediated membrane degradation has been functionally associated to axonal degeneration (López-Vales et al., 2008; Ma et al., 2013; Stys and Jiang, 2002). Also, in tumoral cell lines, RIPK1 and RIPK3 activity is associated with ROS production by activation of the NOX1/NADPH oxidase complex, resulting in oxidative damage (Vandenabeele et al., 2010b). The increase in the oxidative tone causes in turn mPTP activation, calcium dys-homeostasis, and further increase in ROS production and ATP depletion (Görlach et al., 2015). The role of calcium dys-homeostasis and oxidative stress have been well documented during axonal degeneration (Villegas et al., 2014), therefore RIPK1 and RIPK3-mediated ROS production and oxidative damage after an excitotoxic stimuli are likely executors of neurite degeneration.

RIPK3 activity lead to MLKL phosphorylation. In turn, phosphorylated MLKL induces calcium overloading and osmotic stress by opening of Trpm7 channel and the formation of the “MLKL channel” (Cai et al., 2013; Chen et al., 2014). As both MLKL and Trpm7 are expressed in neurons (Bae and Sun, 2011; Liu et al., 2014b), they correspond to possible mediators of necroptotic calcium dys-homeostasis and plasma membrane breakdown during axonal degeneration after glutamate excitotoxicity. In addition, MLKL activation in cell lines leads to mitochondrial fragmentation and depolarization, mPTP formation and ROS production, leading to ATP depletion and calcium dys-homeostasis (Wang et al., 2012).

Our present results show that RIPK1, RIPK3 and MLKL are key players of a necroptotic-like cascade triggered by glutamate excitotoxicity leading to neurite degeneration in hippocampal neurons. Together our work offers a mechanistic explanation for glutamate-induced axonal degeneration that might contribute to loss of neuronal function in neurodegenerative conditions in which the excitotoxic process acts as a primary or secondary neurodegenerative stimulus, unveiling novel therapeutic targets for nervous system disorders. Subsequent studies will be required to show the possible participation of a similar necroptotic mechanism in axonal degeneration triggered by other pro-degenerative stimuli.

Materials and methods

Bioethics

Experiments and animal handling protocols were performed under the approval of the institutional internal bioethics committee and complied with National Institutes of Health (NIH) guidelines.

Drugs, reagents, probes and plasmids

Neurobasal™ medium, Dulbecco's Modified Eagles Medium (DMEM), fetal bovine serum (FBS), B27® supplement (B-27), GlutaMAX™ I, penicillin-streptomycin (P/S), 2.5% Trypsin 10X, Hank's Balanced Salt Solution (HBSS), Hank's Balanced Salt Solution no-calcium no-magnesium (HBSS -Ca^{2+}/-Mg^{2+}), DAPI (358/461 nm), propidium iodide (PI; 535/617 nm), hoechst 33342 (hoechst; 350/461 nm), fura2-AM (340-380/510 nm), fluo4-AM (494/516 nm), F-127, tetramethylrhodamine methyl ester (TMRM; 549/573 nm), calcein-AM (494/517 nm), MitoTracker Red CMXRos (mitotracker; 579/599 nm), were purchased form Thermo Fisher (Waltham, MA, USA). Paraformaldehyde, Poly-L-lysine hydrobromide (PLL), cytosine β-D-arabinofuranoside hydrochloride (AraC), HEPES, cold-fish gelatin, triton-X-100, PMSF, protease inhibitor cocktail P8340 (PIC), L-glutamic acid monosodium salt hydrate (glutamate), necrostatin-1 (nec-1), cyclosporine A (CsA), trypan blue, were purchased from Sigma-Aldrich (St. Louis, MO, USA). Necrostatin-1s (nec-1s) was purchased from BioVision (Milpitas, CA, USA). pLV-RNAi plasmid vector with RIPK3 shRNA and scramble sequences were purchased from Biosettia (San Diego, CA, USA). Fluoromont-G was purchased from Electron Microscopy Sciences (Hatfield, PA, USA). Phos-tag™ was purchased from Wako (Osaka, Osaka, Japan). Non-fat dry milk was purchased from Bio-Rad (Hercules, CA, USA). Excitation and emission wavelengths are shown in nm for fluorescent probes.

Primary hippocampal neuron cultures

Hippocampal neurons were obtained from E18 Sprague-Dawley rat embryos hippocampi using a modified version of the protocol described by Kaech and Banker (Kaech and Banker, 2006). Hippocampi were dissected in ice-cold HBSS -Ca^{2+}/-Mg^{2+} (plus 10 mM HEPES, pH 7.3), treated with 0.25 % Trypsin, washed in plating media (5% FBS DMEM) and dissociated using a fire-polished Pasteur pipettes. Dissociated neurons density and viability was measured using a Neubauer-improved hemocytometer (Marienfield: Lauda-Königshofen, Germany) together with trypan blue dye exclusion

assay, and seeded at the desired density in 0.5 mg/mL PLL treated coverslips (12 or 25 mm; Marienfeld) or plastic dishes (Corning®: Tewksbury, MA, USA) and maintained in a culture chamber with 5 % CO_2 and 37 °C. After 3 hours, the plating media was changed to Neurobasal™ media supplemented with 2% B27, 0.5 mM GlutaMAX™-I and P/S. After three days, a third of the culture media was replaced and treated with 5 µM AraC to inhibit glial cell proliferation. All experiments where done with seven to eight days *in vitro* (7-8DIV) neurons apart from experiments in microfluidic devices that were done with fourteen to fifteen days old cultures (14-15DIV). All experiments with exception of the protein samples for western blots, microfluidic device and the electroporated cultures were performed at a density of 350 cells/mm^2.

Microfluidic devices

Commercial microfluidic devices with 150 µm length microgroove (RD150; Xona Microfluidics, Temecula, CA, USA), were mounted in 25 mm coverslips treated with poly-L-lysine as described before and using the suggested non-plasma bonding protocol provided by the company. Hippocampal neurons were seeded in plating media at 5 × 10^6 cells/mL in the neuronal chamber. The media was changed after three hours for Neurobasal™ supplemented media that was half changed every other day for two weeks. To compartmentalize the axonal treatment, two days before the experiments were performed, a differential volume of media was placed between the neuronal and the axonal compartments (100 and 80 µL in each well, respectively).

Electroporation

After hippocampal dissociation 1× 10^6 hippocampal cells were re-suspended in 100 µL free-serum plating media plus 100 µg of DNA plasmid construct and placed in electroporation cuvettes (2 mm gap; NEPAGENE, Chiba, Japan). The impedance for each electroporation cuvette preparation was adjust between 30 and 40 Ω by free-serum media addition and then subjected to three positive polarity poring pulses (275 V, 2 ms duration, 10 ms decay) separated each one by 50 ms, and five consecutive alternating polarity transfer pulses (20 V, 50 ms duration, 40 ms decay) separated each one by 50 ms, using a NEPA21 Super Electroporator (NEPAGENE). After electroporation, each preparation was re-suspended in fresh plating media and seeded in six 25 mm coverslips previously treated with poly-L-lysine and maintained for regular hippocampal neuron cultures as described before. The electroporation efficiency was approximately 30-40 %.

The four plasmids for shRNA and one scramble sequences for RIPK3 knock down and control respectively, were designed by Biosettia (San Diego, CA, USA) using the *Rattus norvegicus* RIPK3 mRNA sequence (NCBI reference sequence NM_139342.1) and placed in a pRNAi vector that co-express GFP as reporter gene. *ripk3* gene shRNA oligo sequences were:
AAAAGGAAAGGCTTCTAAAGCAATTGGATCCAATTGCTTTAGAAGCCTTTCC;
AAAAGGAAGCATCATTTGGGCATTTGGATCCAAATGCCCAAATGATGCTTCC;
AAAAGGAAGAAACAGCAATCCTTTTGGATCCAAAAGGATTGCTGTTTCTTCC;
AAAAGCCTACAGTCTATTGTCTTTTGGATCCAAAAGACAATAGACTGTAGGC, and the scramble

sequence: AAAAGCTACACTATCGAGCAATTTTGGATCCAAAATTGCTCGATAGTGTAGC. Underlined parts of the sequences highlight the siRNA sequence for each oligo RNA. For RIPK3 shRNA electroporation a mix with equal parts of the four shRNA plasmid vectors were used.

Virion production and lentivirus transduction

Human embryonic kidney 293T cells (ATCC) were transfected into 15 cm^2 dishes using the calcium chloride (1.25 M) method. Media was replaced 4 hours after the initial transfection, and 48 hours later lentivirus enriched media were collected and cleared by slow speed centrifugation at 1,500 rpm for 5 minutes. Subsequently, the conditioned media was filtered through a 0.45-µm pore conic tube filter. The lentiviruses were concentrated using the Lenti-X-concentrator™ reagent (Clontech: Mountainview, CA, USA) and then stored at -80°C.

Hippocampal neuron primary cultures were infected , 3 hours after the neuronal seeding step with 1:10 dilution of shRNA expressing lentiviruses mix in supplemented neurobasal media

Four plasmids for lentiviral transduction of RIPK3 shRNA, were designed by Biosettia using the *Rattus norvegicus* RIPK3 mRNA sequence (NCBI reference sequence NM_139342.1) and cloned in a pLV-RNAi vector that co-express GFP as reporter gene. The *ripk3* shRNA oligo vector used sequences are: GAAAGGCTTCTAAAGCAA; GAAGCATCATTTGGGCAT; GAAGAAACAGCAATCCTT ; CCTACAGTCTATTGTCTT. One plasmid for lentiviral transduction of MLKL shRNA, were designed and packaged by Vigene Bioscience using the *Rattus norvegicus* MLKL mRNA sequence (NCBI reference sequence XM_008772571.2) and cloned in a pLV-RNAi vector that co-express GFP as reporter gene. The *mlkl* shRNA oligo vector used sequences are: GACCAAACTGAAGACAAATAA; TCCCAACATCCTGCGTATATT. One plasmid for lentiviral transduction of scramble shRNA, were designed Vigene Bioscience/ and cloned in a pLV-RNAi vector that co-express GFP as reporter gene.

Immunofluorescence staining

Coverslips were washed twice with 1X PBS solution at room temperature, fixed in 4 % paraformaldehyde for fifteen minutes, washed 3 times with 1X PBS for five minutes, and placed in blocking-permeabilizing solution (BP; 5% cold-fish gelatin; 0.1% Tritón-X-100) for 1 hour. Primary antibody incubation was made over-night in the same BP solution. After 3 x 15 minutes washing steps using 1X PBS, secondary antibodies were diluted in BP solution and incubated for one hour followed by 3 x 15 minutes washing steps using 1X PBS. Each immunofluorescent preparation was mounted after a fast washing step using tri-distillated water in Fluoromont-G with the addition of 3 µM DAPI for some preparations. The antibodies used and dilutions were as follows: mouse anti-acetylated tubulin (AcTub; 1:1000; Sigma-Aldrich), chicken anti- neurofilament medium polypeptide (NF-M; 1:1000; Chemicon – Thermo Fisher), rabbit anti-GFP (GFP; 1:500; Thermo Fisher), rabbit anti-phospho-(S345)-MLKL (pMLKL; 1:500; Abcam: Cambridge, MA, USA), mouse anti-TAU1 (1:500; Millipore: Burlington, MA, USA), rabbit anti-MAP2 (MAP2; 1:1000; Millipore), goat anti-mouse alexa 488 (1:1000; Thermo Fisher), goat anti-rabbit alexa 488 (1:1000; Thermo Fisher), goat anti-rabbit alexa 546 (1:1000; Thermo Fisher); goat anti-chicken alexa 594 (1:1000), donkey anti-mouse alexa 594 (1:1000; Thermo Fisher).

Images were acquired in an Olympus IX81-DSU microscope (Olympus: Shinjuku, Tokyo, Japan) equipped with an Orca-R^2 camera (Hamamatsu: Hamamatsu City, Shizuoka, Japan) and Xcellence software (Olympus). Image quantification was made using the ImageJ software (NIH: Bethesda, Maryland, USA).

Neurite and axonal integrity index

Neurite integrity index quantification was made to evaluate the amount of damage over the NF-M cytoskeleton using images acquired with 100X (regular culture) or 60X (microfluidic culture) objectives. All NF-M immunofluorescence images were processed simultaneously for each experiment using ImageJ, to generate binarized masks that were subjected to particle analysis using filters of 0.3 µm^2 for noise signal elimination (**Fig. S2A**). Particles with 25 µm^2 or lower area and 0.8 or more circularity index values were considered as degenerated neurites as they correspond to NF-M positive neurite fragments. Particles with values higher than 25 µm^2 of area and 0.8 or less circularity index were classified as non-degenerated NF-M positive neurites. The neurite integrity index was quantified as the ratio between the non-degenerated and total NF-M stained area. The same NF-M image processing and quantification protocol was used for the axonal integrity index (**Fig. 4**).

TAU1 puncta quantification

TAU1 puncta quantification was performed by generating a 2000 µm^2 grid (ImageJ) over TAU1 images taken with a 40X objective (**Fig. S1E)**. For each picture, 5 random grid-squares with similar axon density were used for quantification of the number of puncta/2000 µm^2 (**Fig. S1F**). Co-localization with MAP2 immunofluorescent stain and DAPI nuclear stain were used to ignore dendritic neurites and neuronal somas from the quantification.

TUNEL and propidium iodide (PI) exclusion assay

TUNEL assay was performed using the Click-iT® TUNEL Alexa Fluor® 488 Imaging Assay (Thermo Fisher) according to manufacturer protocol for fluorescence microscopy. Simultaneous TUNEL and immunofluorescent staining for AcTub was performed according to the protocol provided. Images were acquired using an Olympus IX81-DSU microscope. Image processing and quantification were made using ImageJ. For the PI exclusion assay, live-cell hippocampal neuronal cultures were washed twice with HBSS (10 mM HEPES, pH 7.42) and exposed to the same HBSS solution plus 1 µM Hoechst and 15 µM PI for twenty minutes at 37 °C. Samples were washed twice and mounted in a Chamlide® (Live Cell Insturment: Nowon gu, Seul, Korea) recording chamber in HBSS. Live-cell snap-shot images were acquired using an Olympus IX81-DSU microscope. Image processing and quantification were made using the ImageJ software.

Electron microscopy

Hippocampal neuronal cultures seeded in plastic dishes were washed twice with PBS 1X at 37 °C, and fixed in 3% glutaraldehyde (Sigma-Aldrich) diluted in sodium cacodylate buffer (50 mM sodium cacodylate, pH 7.3; Sigma-Aldrich) for two hours at room temperature. Samples were post-fixed in 3 %

potassium ferrocyanide diluted in osmium tetra-oxide solution (reduced for thirty minutes at room temperature), stained with 2 % uranyl acetate solution, and dehydrated with a gradient of ethanol solutions (30, 50 and 70%) five minutes each, and finally three times with 100% ethanol for ten minutes. The dehydrated samples were included in epoxy resin and cured at 60 °C overnight. Included samples were added to pre-crafted epoxy resin blocks and cut in sections of 50 – 80 nm with an ultra-microtome and mounted in copper grids. Images were acquired in a TECNAI 12 BIOTWIN transmission electron microscope (FEI: Hillsboro, OR, USA). Image processing was made using ImageJ.

Western blot

Triplicate protein samples from hippocampal neuronal cultures seeded in plastic dishes at 526 cell/mm^2, were collected in ice-cold RIPA buffer (150 mM NaCl, 50 mM Tris-HCl, 1% NP-40, 0.5 % sodium deoxycholate acid, 0.1% sodium dodecyl sulfate, pH 7.6; Sigma-Aldrich) plus 1 mM PMSF, PIC and phosphatase inhibitors (1 mM NaF, 5 mM Na_3VO_4). All protein samples and processing were managed in EDTA free-buffer due to incompatibility of EDTA with the PhosTag™ procedure for phosphorylated protein mobility shift assay. Protein samples were centrifuged for fifteen minutes at 14000 g and 4 °C, the soluble fraction was collected, and the protein concentration was estimated using the BCA Protein Assay™ (Pierce, Thermo Fisher). Protein samples were diluted in 5X sample buffer, boiled for 5 minutes, and 20 µg of protein were loaded in 10% SDS-PAGE gels with or without 50 µM Phostag™ and 100 µM $MnCl_2$, subjected to gel electrophoresis, and then transferred to PVDF membranes (Thermo Scientific) for western blotting. For RIPK1 western blots and before the transference step, all gels were subjected to a ten minutes wash in 1 mM EDTA transfer buffer for Mn^{2+} elimination, followed by a ten-minute wash in EDTA-free transfer buffer. The protein transferred membranes were incubated for one hour in blocking solution (5 % non-fat dry milk; 0.1% tween 20; PBS 1X) at room-temperature, incubated over-night at 4 °C in primary antibody solution, washed three times in T-PBS 1X solution (0.1% tween 20), incubated for one hour in HRP secondary antibody solution, washed three times with T-PBS 1X, and revealed using picogram or femtogram sensitive ECL reactives (Thermo Scientific) and photosensitive films (Fujifilm: Tokio, Japan). Primary and secondary antibodies were diluted in blocking solution and the dilution used were as follows: 1:400 mouse anti-RIPK1 (BD Pharmigen, San Jose, CA, USA), rabbit anti-phospho-(S345)-MLKL (pMLKL; 1:500; Abcam: Cambridge, MA, USA), rabbit anti-phospho-(S232)-RIPK3 (pRIPK3; 1:1000; Abcam), 1:200 rabbit anti-RIPK3 (IMGENEX: San Diego, CA, USA), 1:300 mouse anti-Hsp90 (Santa Cruz Biotechnology: TX, USA), 1:5000 goat anti-mouse HRP (Bio-Rad), 1:10000 goat anti-rabbit HRP (Bio-Rad) Thermo Scientific Page Ruler Pre-stained Protein Ladder was used as molecular weight standard (Thermo-Fisher) in all gels with exception of gels with the Phostag™ additive were proteins does not migrate accordingly their molecular weight.

Immunoprecipitation

Immunoprecipitation experiments were performed by incubating 100 µg of protein with 2.5 µg of anti-RIPK1 (Cell Signaling: Danvers, MA, USA) with rotation at 4 °C for 48 h. Then, 50 µL of protein G magnetic beads (Biorad) were added to each sample and incubated with rotation at 4 °C for 3 h.

Following magnetic separation, beads were mixed with loading buffer and boiled at 90 °C for 5 min. After the elution step, samples were analyzed by western blotting.

Non-quenching TMRM imaging and mPTP activation assay

For live-cell imaging of mitochondrial potential in neurite mitochondria, hippocampal neuronal cultures were washed twice with HBSS solution and treated with 50 nM TMRM diluted in HBSS for fifteen minutes at 37°C. Samples were mounted in the same 50 nM TMRM HBSS solution in a Chamlide® recording chamber and subjected to snap-shot image acquisition with an Olympus IX81-DSU microscope. Image processing and quantification were made using ImageJ software. TMRM experiments in compartmentalized cultures were performed in equivalent experimental conditions but using a Leica Dmi8 microscope (Wetzlar, Germany).

Mitochondrial potential transition pore (mPTP) opening was evaluated using the Image-IT™ LIVE Mitochondrial Transition Pore Assay Kit (Thermo Fisher) according to the manufacturer protocol. Cobalt ion (Co^{2+}) quenches calcein fluorescence, which is only retained in Co^{2+} impermeable compartments as mPTP-closed mitochondria. After mPTP opening, Co^{2+} enters mitochondria and calcein fluorescence is quenched in this organelle. Mitotracker is used as mPTP independent mitochondrial stain and to discard non-mitochondrial calcein staining. Hippocampal neuronal cultures were washed twice with HBSS solution and treated in the same solution with 1 µM Calcein-AM, 1 mM $CoCl_2$, 200 nM mitotracker for thirty minutes at 37°C. Samples were washed twice with fresh HBSS, mounted in a Chamlide® recording chamber with HBSS and subjected to snap-shot image acquisition with an Olympus IX81-DSU microscope (Olympus). Image processing and quantification were made using ImageJ software with a co-localization free available plugin from Pierre Bourdoncle (Paris, France).

Calcium imaging

For live-cell free intracellular Ca^{2+} imaging, hippocampal neuronal cultures were loaded with 1 µM Fura2-AM in HBSS solution plus 0.02% F-127 for thirty minutes at 37°C. Samples were washed twice and mounted in a Chamlide® recording chamber with HBSS. Fura2 340 and 380 nm excitation time-lapse recordings were acquired for 100 minutes with 0.5 Hz frequency the first 15 minutes and with 0.1 Hz for the 85 minutes left, to record the initial fast and later slow calcium dynamics induced by the glutamate stimulus, respectively. Images were acquired, processed for the 340/380 ratio and analyzed with an Olympus IX81-DSU microscope equipped with an Orca-R^2 camera and Xcellence software. Time-lapse calcium dynamics are shown as averaged time-lapse traces of neurites (**Fig. 8B**) or neurons (**Fig. S6B**). Records were obtained with a n = 3, meaning three different cultures, with 3 repetitions for each n. ROI's where defined in Xcellence software by drawing by hand following the shape of isolated neurites for the neurite recordings (**Fig. 8A**), or using circular shaped ROI's for neuronal soma recordings (**Fig. S6A**).

Equivalent procedure was used for experiments in compartmentalized cultures but using fluo4 as live-cell free intracellular Ca^{2+} probe. Axons in the axonal compartment of each microfluidic device were loaded with 4 µM solution of fluo4-AM in HBSS solution. Snapshots were taken before (1 minutes) or

after 30, 60 and 90 minutes of glutamate treatment (minute 3), in the same field of view for each compartmentalized culture using the same microscope, camera and light exposure configurations. Each treatment time point was normalized by the mean time zero fluorescence value. Images were acquired with a Nikon Ti2-E inverted microscope equipped with an C2-DU3 3PMT (Nikon: Tokyo, Japan) and NIS-Elements software. Image processing and quantification were made using ImageJ software.

Data analysis and statistics

Data analysis and statistics were performed in Prism® software (Graphpad Software: La Jolla, CA, USA) Data is expressed as mean ± S.E.M. n = 3 refers to the number of independent cultures made for each experiment, with exception of experiments in microfluidics devices, where each n refers to one microfluidic culture. Data were checked for normality (non-significant Shapiro-Wilk normality test; Skewness = $-2 < 0 < 2$; and Kurtosis = $-7 < 0 < 7$). Parametric statistical analyses were performed using t-Test for comparison of two treatments, and one-way ANOVA for multiple treatments. Two-way ANOVA were used for multiple variable analysis in calcium dynamic experiments. P values < 0.05 were considered as significant. Tukey's and Bonferroni's post-test where used for one-way ANOVA and two-way ANOVA respectively for determining differences between groups. Non-parametric data was analyzed with Kurskal-Wallis Test. Differences within groups for non-parametric data were checked with Dunn's multiple comparison test.

Acknowledgements

We thank Monica Perez for excellent EM processing and Ximena Vergés and Ramon Ramirez for the assistance in the time-lapse experiments.

Competing interests

No competing interests declared.

Funding

This work was supported by Comisión Nacional de Investigación Científica y Tecnológica (CONICYT; 2009 fellowship for PhD studies in Chile), and by grants from Geroscience Center for Brain Health and Metabolism (FONDAP-15150012), Fondo Nacional de Desarrollo Científico y Tecnológico (FONDECYT: 1070377 (FC); FONDECYT 1171137 (FB)), Millennium Nucleus RC120003 and Ring Initiative ACT1109 (FC), Basal Center of Excellence in Science and Technology (AFB 170005 (FB)).

References

Adalbert, R., Nogradi, A., Babetto, E., Janeckova, L., Walker, S. A., Kerschensteiner, M., Misgeld, T. and Coleman, M. P. (2009). Severely dystrophic axons at amyloid plaques remain continuous and connected to viable cell bodies. *Brain* **132**, 402–416.

Ankarcrona, M., Dypbukt, J. M., Bonfoco, E., Zhivotovsky, B., Orrenius, S., Lipton, S. a and Nicotera, P. (1995). Glutamate-induced neuronal death: a succession of necrosis or apoptosis depending on mitochondrial function. *Neuron* **15**, 961–73.

Ashpole, N. M. and Hudmon, A. (2011). Excitotoxic neuroprotection and vulnerability with CaMKII inhibition. *Mol. Cell. Neurosci.* **46**, 720–730.

Avery, M. a, Rooney, T. M., Pandya, J. D., Wishart, T. M., Gillingwater, T. H., Geddes, J. W., Sullivan, P. G. and Freeman, M. R. (2012). WldS prevents axon degeneration through increased mitochondrial flux and enhanced mitochondrial Ca2+ buffering. *Curr. Biol.* **22**, 596–600.

Bae, C. Y. and Sun, H. (2011). TRPM7 in cerebral ischemia and potential target for drug development in stroke. *Acta Pharmacol. Sin.* **32**, 725–733.

Barrientos, S. a, Martinez, N. W., Yoo, S., Jara, J. S., Zamorano, S., Hetz, C., Twiss, J. L., Alvarez, J. and Court, F. A, (2011). Axonal degeneration is mediated by the mitochondrial permeability transition pore. *J. Neurosci.* **31**, 966–978.

Brenner, D., Blaser, H. and Mak, T. W. (2015). Regulation of tumour necrosis factor signalling: live or let die. *Nat. Rev. Immunol.* **15**, 362–374.

Caccamo, A., Branca, C., Piras, I. S., Ferreira, E., Huentelman, M. J., Liang, W. S., Readhead, B., Dudley, J. T., Spangenberg, E. E., Green, K. N., et al. (2017). Necroptosis activation in Alzheimer's disease. *Nat. Neurosci.* **20**, 1236–1246,

Cai, Z., Jitkaew, S., Zhao, J., Chiang, H.-C., Choksi, S., Liu, J., Ward, Y., Wu, L. and Liu, Z.-G. (2013). Plasma membrane translocation of trimerized MLKL protein is required for TNF-induced necroptosis. *Nat. Cell Biol.* **16**, 55–65.

Calixto, A., Jara, J. S. and Court, F. A. (2012). Diapause formation and downregulation of insulin-like signaling via DAF-16/FOXO delays axonal degeneration and neuronal loss. *PLoS Genet.* **8**, 1–15.

Chavez-Valdez, R., Martin, L. J., Flock, D. L. and Northington, F. J. (2012). Necrostatin-1 attenuates mitochondrial dysfunction in neurons and astrocytes following neonatal hypoxia-ischemia. *Neuroscience* **219**, 192–203.

Chen, W., Zhou, Z., Li, S., Zhong, C. Q., Zheng, X., Wu, X., Zhang, Y., Ma, H., Huang, D., Li, W., et al. (2013). Diverse sequence determinants control human and mouse receptor interacting protein 3 (RIP3) and mixed lineage kinase domain-like (MLKL) interaction in necroptotic signaling. *J. Biol. Chem.* **288**, 16247–16261.

Chen, X., Li, W., Ren, J., Huang, D., He, W.-T., Song, Y., Yang, C., Li, W., Zheng, X., Chen, P., et al. (2014). Translocation of mixed lineage kinase domain-like protein to plasma membrane leads to necrotic cell death. *Cell Res.* **24**, 105–121.

Chen, Y., Zhang, L., Yu, H., Song, K., Shi, J., Chen, L. and Cheng, J. (2018). Necrostatin-1 Improves Long-term Functional Recovery Through Protecting Oligodendrocyte Precursor Cells After Transient Focal Cerebral Ischemia in Mice. *Neuroscience* **371**, 229–241.

Coleman, M. P. and Freeman, M. R. (2010). Wallerian degeneration, wld(s), and nmnat. *Annu. Rev. Neurosci.* **33**, 245–267.

Coleman, M. P. and Perry, V. H. (2002). Axon pathology in neurological disease: a neglected therapeutic target. *Trends Neurosci.* **25**, 532–537.

Conforti, L., Gilley, J. and Coleman, M. P. (2014). Wallerian degeneration: an emerging axon death pathway linking injury and disease. *Nat. Rev. Neurosci.* **15**, 394–409.

Diprospero, N. A., Chen, E. Y., Charles, V., Plomann, M., Kordower, J. H. and Tagle, D. A. (2004). Early changes in Huntington's disease patient brains involve alterations in cytoskeletal and synaptic elements. *J. Neurocytol.* **33**, 517–533.

Dong, K., Zhu, H., Song, Z., Gong, Y., Wang, F., Wang, W., Zheng, Z., Yu, Z., Gu, Q., Xu, X., et al. (2012). Necrostatin-1 protects photoreceptors from cell death and improves functional outcome after experimental retinal detachment. *Am. J. Pathol.* **181**, 1634–1641.

Fischer, L. R., Culver, D. G., Tennant, P., Davis, A. A., Wang, M., Castellano-Sanchez, A., Khan, J., Polak, M. A. and Glass, J. D. (2004). Amyotrophic lateral sclerosis is a distal axonopathy: Evidence in mice and man. *Exp. Neurol.* **185**, 232–240.

Görlach, A., Bertram, K., Hudecova, S. and Krizanova, O. (2015). Calcium and ROS: A mutual interplay. *Redox Biol.* **6**, 260–271.

Hosie, K. a, King, A. E., Blizzard, C. a, Vickers, J. C. and Dickson, T. C. (2012). Chronic excitotoxin-induced axon degeneration in a compartmented neuronal culture model. *ASN Neuro* **4**, 47–57.

Ikegami, K. and Koike, T. (2003). Non-apoptotic neurite degeneration in apoptotic neuronal death: pivotal role of mitochondrial function in neurites. *Neuroscience* **122**, 617–626.

Ito, Y., Ofengeim, D., Najafov, A., Das, S., Saberi, S., Li, Y., Hitomi, J., Zhu, H., Chen, H., Mayo, L., et al. (2016). RIPK1 mediates axonal degeneration by promoting inflammation and necroptosis in ALS. *Science.* **353**, 603–608.

Kaczmarek, A., Vandenabeele, P. and Krysko, D. V. (2013). Necroptosis: the release of damage-associated molecular patterns and its physiological relevance. *Immunity* **38**, 209–223.

Kaech, S. and Banker, G. (2006). Culturing hippocampal neurons. *Nat. Protoc.* **1**, 2406–2415.

Lau, A. and Tymianski, M. (2010). Glutamate receptors, neurotoxicity and neurodegeneration. *Pflugers Arch.* **460**, 525–542.

Li, Y., Yang, X., Ma, C., Qiao, J. and Zhang, C. (2008). Necroptosis contributes to the NMDA-induced excitotoxicity in rat's cultured cortical neurons. *Neurosci. Lett.* **447**, 120–123.

Lingor, P., Koch, J. C., Tönges, L. and Bähr, M. (2012). Axonal degeneration as a therapeutic target in the CNS. *Cell Tissue Res.* **349**, 289–311.

Liu, M., Wu, W., Li, H., Li, S., Huang, L., Yang, Y., Sun, Q., Wang, C., Yu, Z. and Hang, C. (2014a). Necroptosis, a novel type of programmed cell death, contributes to early neural cells damage after spinal cord injury in adult mice. *J. Spinal Cord Med.* **38**, 745–753.

Liu, S., Wang, X., Li, Y., Xu, L., Yu, X., Ge, L., Li, J., Zhu, Y. and He, S. (2014b). Necroptosis Mediates TNF-Induced Toxicity of Hippocampal Neurons. *Biomed Res. Int.* **2014**, 1–11.

López-Vales, R., Navarro, X., Shimizu, T., Baskakis, C., Kokotos, G., Constantinou-Kokotou, V., Stephens, D., Dennis, E. A. and David, S. (2008). Intracellular phospholipase A2 group IVA and group VIA play important roles in Wallerian degeneration and axon regeneration after peripheral nerve injury. *Brain* **131**, 2620–2631.

Ma, M., Ferguson, T. a, Schoch, K. M., Li, J., Qian, Y., Shofer, F. S., Saatman, K. E. and Neumar, R. W. (2013). Calpains mediate axonal cytoskeleton disintegration during Wallerian degeneration. *Neurobiol. Dis.* **56**, 34–46.

Mehta, A., Prabhakar, M., Kumar, P., Deshmukh, R. and Sharma, P. L. (2013). Excitotoxicity: bridge to various triggers in neurodegenerative disorders. *Eur. J. Pharmacol.* **698**, 6–18.

Neukomm, L. J., Burdett, T. C., Seeds, A. M., Hampel, S., Coutinho-Budd, J. C., Farley, J. E., Wong, J., Karadeniz, Y. B., Osterloh, J. M., Sheehan, A. E., et al. (2017). Axon Death Pathways Converge on Axundead to Promote Functional and Structural Axon Disassembly. *Neuron* **95**, 78–91.

Nomura, M., Ueno, A., Saga, K., Fukuzawa, M. and Kaneda, Y. (2014). Accumulation of cytosolic calcium induces necroptotic cell death in human neuroblastoma. *Cancer Res.* **74**, 1056–1066.

Ofengeim, D., Ito, Y., Najafov, A., Zhang, Y., Shan, B., DeWitt, J. P., Ye, J., Zhang, X., Chang, A., Vakifahmetoglu-Norberg, H., et al. (2015). Activation of necroptosis in multiple sclerosis. *Cell Rep.* **10**, 1836–1849.

Osterloh, J. M., Yang, J., Rooney, T. M., Fox, A. N., Adalbert, R., Powell, E. H., Sheehan, A. E., Avery, M. A., Hackett, R., Logan, M. A., et al. (2012). dSarm/Sarm1 Is Required for Activation of an Injury-Induced Axon Death Pathway. *Science (80-.).* **337**, 481–484.

Rodriguez, D., Weinlich, R., Brown, S., Guy, C., Fitzgerald, P., Dillon, C., Oberst, A., Quarato, G., Low, J., Cripps, J., et al. (2015). Characterization of RIPK3-mediated phosphorylation of the activation loop of MLKL during necroptosis. *Cell Death Differ.* **23**, 76–88.

Rosenbaum, D. M., Degterev, A., David, J., Rosenbaum, P. S., Roth, S., Grotta, J. C., Cuny, G. D., Yuan, J. and Savitz, S. I. (2010). Necroptosis, a novel form of caspase-independent cell death, contributes to neuronal damage in a retinal ischemia-reperfusion injury model. *J. Neurosci. Res.* **88**, 1569–1576.

Salvadores, N., Sanhueza, M., Manque, P. and Court, F. A. (2017). Axonal Degeneration during Aging and Its Functional Role in Neurodegenerative Disorders. **11**,1–21.

Shang, L., Huang, J.-F., Ding, W., Chen, S., Xue, L.-X., Ma, R.-F. and Xiong, K. (2014). Calpain: a molecule to induce AIF-mediated necroptosis in RGC-5 following elevated hydrostatic pressure. *BMC Neurosci.* **15**, 1–11.

Sosna, J., Voigt, S., Mathieu, S., Lange, A., Thon, L., Davarnia, P., Herdegen, T., Linkermann, A., Rittger, A., Chan, F. K. M., et al. (2014). TNF-induced necroptosis and PARP-1-mediated necrosis represent distinct routes to programmed necrotic cell death. *Cell. Mol. Life Sci.* **71**, 331–348.

Stirling, D. P. and Stys, P. K. (2010). Mechanisms of axonal injury: internodal nanocomplexes and calcium deregulation. *Trends Mol. Med.* **16**, 160–170.

Stys, P. K. and Jiang, Q. (2002). Calpain-dependent neurofilament breakdown in anoxic and ischemic rat central axons. *Neurosci. Lett.* **328**, 150–154.

Tagliaferro, P. and Burke, R. E. (2016). Retrograde Axonal Degeneration in Parkinson Disease. *J. Parkinsons. Dis.* **6**, 1–15.

Takahashi, N., Duprez, L., Grootjans, S., Cauwels, a, Nerinckx, W., DuHadaway, J. B., Goossens, V., Roelandt, R., Van Hauwermeiren, F., Libert, C., et al. (2012). Necrostatin-1 analogues: critical issues on the specificity, activity and in vivo use in experimental disease models. *Cell Death Dis.* **3**, 1–10.

Thein, S., Tao-Cheng, J. H., Li, Y., Ulrich Bayer, K., Reese, T. S. and Dosemeci, A. (2014). CaMKII mediates recruitment and activation of the deubiquitinase CYLD at the postsynaptic density.

PLoS One **9**, 1–9.

Vandenabeele, P., Declercq, W., Van Herreweghe, F. and Vanden Berghe, T. (2010a). The role of the kinases RIP1 and RIP3 in TNF-induced necrosis. *Sci. Signal.* **3**,1–8.

Vandenabeele, P., Galluzzi, L., Vanden Berghe, T. and Kroemer, G. (2010b). Molecular mechanisms of necroptosis: an ordered cellular explosion. *Nat. Rev. Mol. Cell Biol.* **11**, 700–714.

Vargas, M. E., Yamagishi, Y., Tessier-Lavigne, M. and Sagasti, A. (2015). Live Imaging of Calcium Dynamics during Axon Degeneration Reveals Two Functionally Distinct Phases of Calcium Influx. *J. Neurosci.* **35**, 15026–15038.

Vieira, M., Fernandes, J., Carreto, L., Anuncibay-Soto, B., Santos, M., Han, J., Fernández-López, a, Duarte, C. B., Carvalho, a L. and Santos, a E. (2014). Ischemic insults induce necroptotic cell death in hippocampal neurons through the up-regulation of endogenous RIP3. *Neurobiol. Dis.* **68C**, 26–36.

Villegas, R., Martinez, N., Lillo, J., Pihan, P., Hernandez, D., Twiss, J. L. and Court, F. A. (2014). Calcium Release from Intra-Axonal Endoplasmic Reticulum Leads to Axon Degeneration through Mitochondrial Dysfunction. *J. Neurosci.* **34**, 7179–7189.

Wang, Z., Jiang, H., Chen, S., Du, F. and Wang, X. (2012). The mitochondrial phosphatase PGAM5 functions at the convergence point of multiple necrotic death pathways. *Cell* **148**, 228–243.

Wang, Y., Wang, J., Yang, H., Zhou, J., Feng, X., Wang, H. and Tao, Y. (2015). Necrostatin-1 mitigates mitochondrial dysfunction post-spinal cord injury. *Neuroscience* **289**, 224–232.

Wayman, G. A., Lee, Y. S., Tokumitsu, H., Silva, A. and Soderling, T. R. (2008). Calmodulin-Kinases: Modulators of Neuronal Development and Plasticity. *Neuron* **59**, 914–931.

Xu, Y., Wang, J., Song, X., Qu, L., Wei, R., He, F., Wang, K. and Luo, B. (2016). RIP3 induces ischemic neuronal DNA degradation and programmed necrosis in rat via AIF. *Sci. Rep.* **6**, 445-453.

You, Z., Savitz, S. I., Yang, J., Degterev, A., Yuan, J., Cuny, G. D., Moskowitz, M. a and Whalen, M. J. (2008). Necrostatin-1 reduces histopathology and improves functional outcome after controlled cortical impact in mice. *J. Cereb. Blood Flow Metab.* **28**, 1564–1573.

Figures

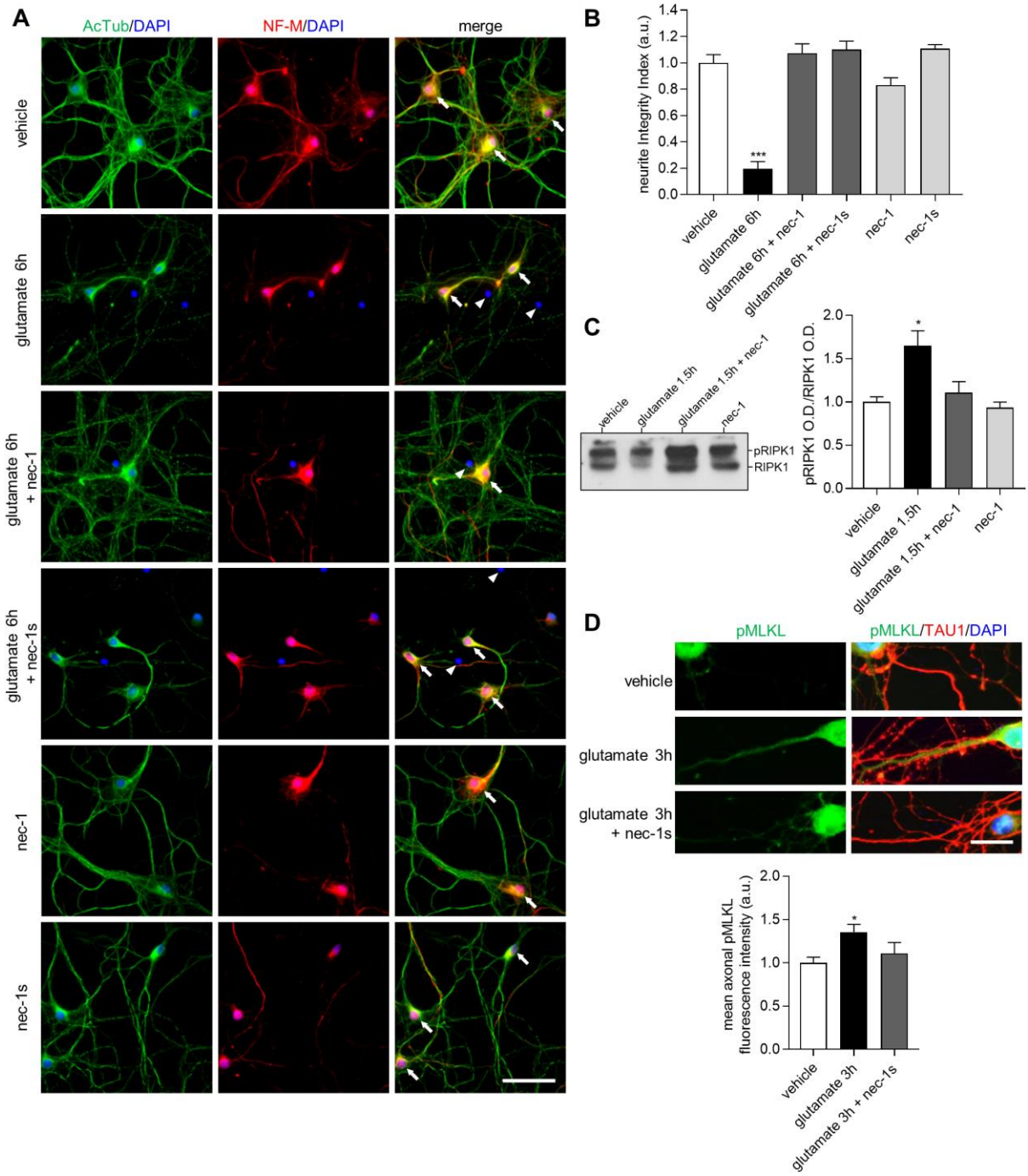

Figure 1. RIPK1 inhibition delays neurite degeneration in cultured hippocampal neurons exposed to glutamate and prevents RIPK1 and MLKL phosphorylation induced by glutamate. (**A**) Dissociated 7-8DIV cultured hippocampal neurons immunostained for acetylated tubulin (Ac-Tub, green), neurofilament medium polypeptide (NF-M, red) and DAPI nuclear staining (blue). Cultures were treated with vehicle or glutamate (20 µM for 6 hours) with or without nec-1 or nec-1s pre-treatment (100 µM for 18 hours). Arrows and arrowhead indicate healthy and condensed neuronal somas, respectively. Scale bar, 50 µm. (**B**) Quantification of neurite integrity for immunostained neurons as in **Fig. 1A**, using the NF-M mean neurite integrity index ± S.E.M. (n=3; one-way ANOVA, *** $P<0.001$; Tukey's post-test: *** show significant differences compared to the vehicle treatment). (**C**) **Left**: Western-blot of RIPK1 from protein lysates from hippocampal cultures treated with vehicle or glutamate (20 µM for 1.5 hours) with or without nec-1 pre-treatment (100 µM for 18 hours). Phosphorylated (pRIPK1) and un-phosphorylated (RIPK1) bands were visualized using RIPK1 antibody on membranes with proteins transferred from a Phostag™ phosphorylated protein SDS-PAGE shift assay. **Right**: Densitometric analysis of RIPK1 Phostag™ western-blots. The relative amount of pRIPK1 normalized by total amount of RIPK1 (pRIPK1 + RIPK1) ± S.E.M. are shown (n=3; one-way ANOVA, * $P<0.05$; Tukey's post-test: * show significant differences compared to the vehicle treatment). (**D**) **Top**: Dissociated 7-8DIV hippocampal neuron cultures immunostained for pMLKL (green), TAU1 (red; axonal immuno-stain) and DAPI nuclear staining (blue). Cultures were treated with vehicle or glutamate (20 µM for 3 hours) with or without nec-1s pre-treatment (100 µM for 18 hours). Scale bar, 20 µm. Full images of this experiment can be found in **Fig S2C**. **Bottom**: Quantification of the mean axonal immunofluorescence intensity of pMLKL ± S.E.M. (n=3; one-way ANOVA, * $P<0.05$; Tukey's post-test: * show significant differences with vehicle treatment). Quantifications were done from three independent cultures, each one with three replicates for each treatment.

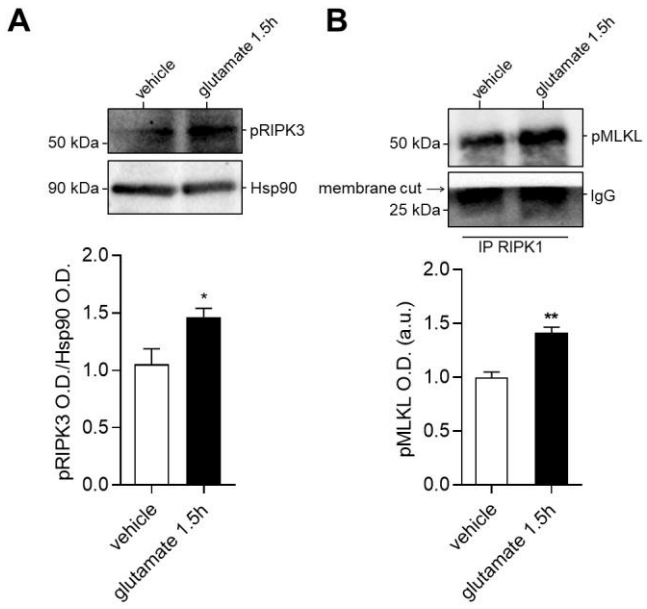

Figure 2. Glutamate treatment of cultured hippocampal neurons induce an increase of RIPK3 phosphorylation and pMLKL co-immunoprecipitation with RIPK1. Dissociated 7-8DIV cultured hippocampal neurons protein lysates were collected after vehicle or glutamate (20 µM glutamate 1.5 hours) treatments and used for western-blot analysis of pRIPK3 and pMLKL. (**A**) **Top**: Western-blot of pRIPK3 and Hsp90 (loading control). **Bottom**: Densitometric quantification of pRIPK3 mean levels normalized by the Hsp90 mean values ± S.E.M. (n = 3, unpaired, two tailed t-Test, * P<0.05). (**B**) **Top**: Western-blot of pMLKL and IgG (loading control) from RIPK1-immunoprecipitated protein samples. **Bottom**: Densitometric quantification of pMLKL mean levels normalized by the IgG mean values ± S.E.M. (n = 3, unpaired, two tailed t-Test, ** P<0.01). Membrane cut site in the IgG western-blot is indicated. Quantifications were done from three independent cultures, each one with three replicates for each treatment.

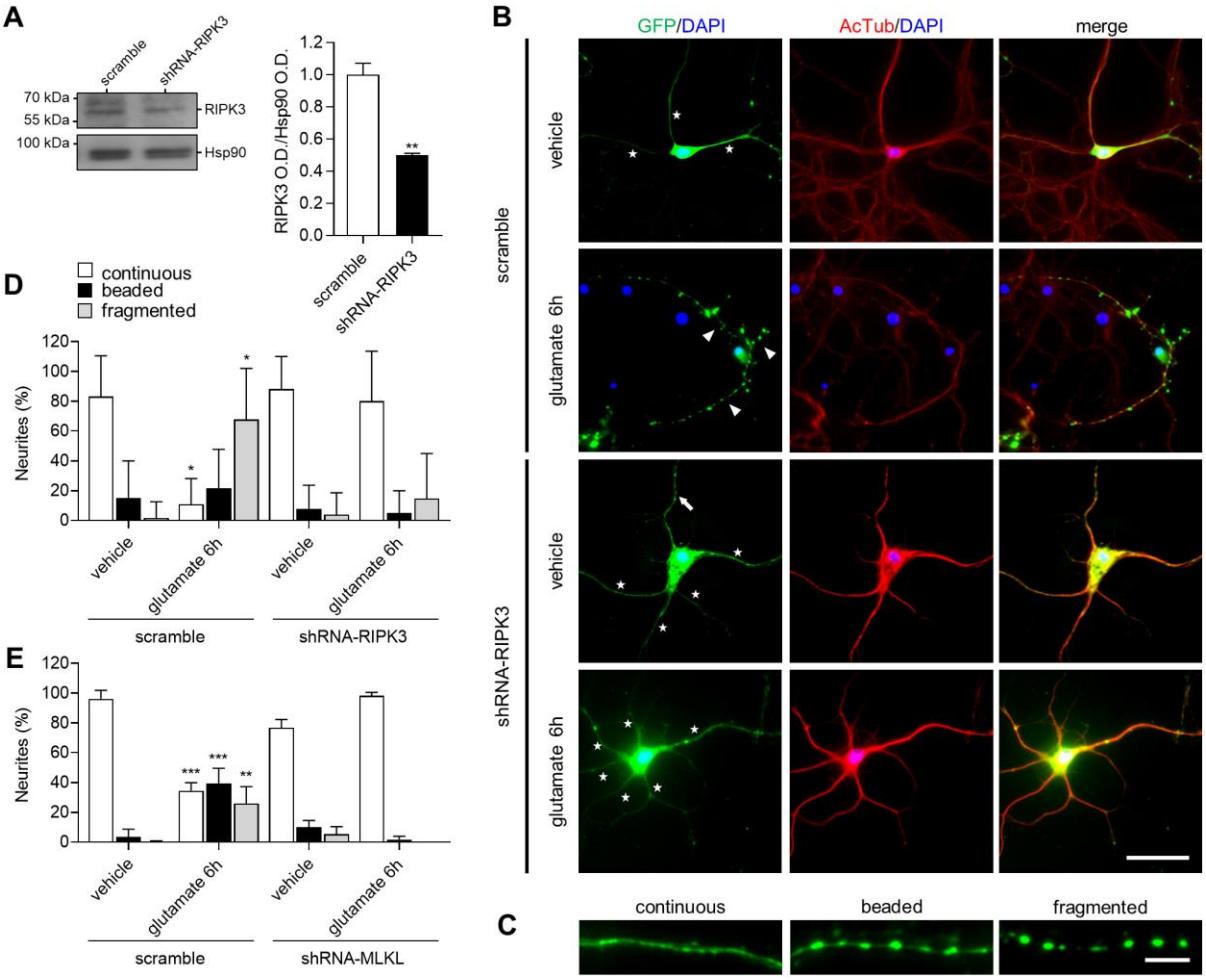

Figure 3. RIPK3 and MLKL knock-down prevent neurite degeneration in hippocampal neurons exposed to glutamate. (**A**) **Left**: RIPK3 western-blot from protein lysates of 7-8DIV hippocampal neuronal cultures electroporated with scramble or shRNA-RIPK3 plasmids (see methods). Hsp90 western-blot was used as loading control for both conditions. **Righ**t: Densitometric analysis of the relative RIPK3 levels normalized by Hsp90 mean values ± S.E.M (n = 3, unpaired, two-tailed, t-Test, **P<0.01). (**B**) Dissociated hippocampal neurons in culture electroporated with scramble or shRNA-RIPK3 plasmids. Neurons were immunostained for GFP (green) and Ac-Tub (red) and with DAPI nuclear staining (blue). Cultures were treated with vehicle or glutamate (20 µM for 6 hours: glutamate 6h). Stars depict the presence of neurites with a continuous morphology, arrows show beaded neurites and arrowheads fragmented neurites. Scale bar, 50 µm. (**C**) Detailed images of GFP positive neurites with continuous, beaded or fragmented morphology. Scale bar, 10 µm. (**D**) Percentage ± S.E.M of neurites from single neurons that show continuous, beaded or fragmented morphology for the treatments described in panel B (n = 3, one-way ANOVA, *P<0.05, *** P<0.001; Tukey's post-test: * and *** show significant differences with vehicle treatment in scramble electroporated neurons). (**D**) Mean percentage ± S.E.M

of neurites from single neurons that show continuous, beaded or fragmented morphology, for the treatments described in **Fig. S4,** that show the effects of MLKL knock-down over glutamate induced neurite degeneration in 7-8DIV cultured hippocampal neurons (n = 3, one-way ANOVA, *P<0.05, *** P<0.001; Tukey's post-test: * and *** show significant differences with vehicle treatment in scramble electroporated neurons). Quantifications were done from three independent cultures, each one with three replicates for each treatment.

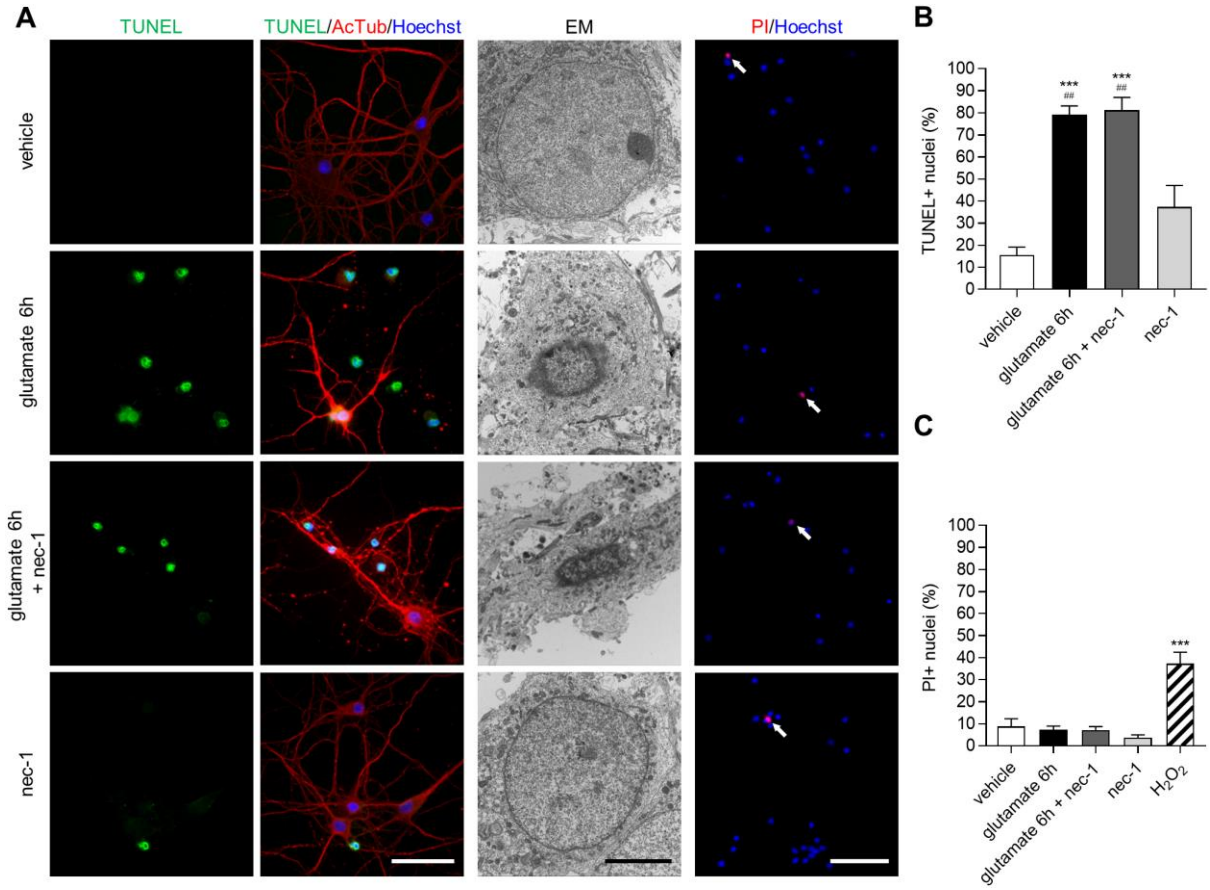

Figure 4. RIPK1 inhibition do not prevent apoptotic neuronal death in cultured hippocampal neurons exposed to glutamate. (**A**) 7-8DIV hippocampal neuron cultures subjected to: **1st and 2nd columns:** TUNEL assay (TUNEL stain (green), hoechst stain (blue), AcTub immuno-stain (red). Scale bar, 50 µm. **3rd column (EM)**: processed for transmission EM. Scale bar, 5 µm. **4th column**: Live-cell PI exclusion assay (PI: red, hoechst: blue). Arrows depict PI positive nuclei. Scale bar, 100 µm. Cultures were treated with vehicle or glutamate (20 µM for 6 hours) treatment with or without nec-1 pre-treatment (100 µM for 18 hours). (**B**) Mean percentage ± S.E.M of TUNEL positive neurons for each treatment as shown in **Fig. 4A** (n = 3, one-way ANOVA, ##P<0.01, ***P<0.001; Tukey's post-test: ***, show significant differences with vehicle treatment; #, show significant differences with nec-1 control treatment). (**C**) Mean percentage ± S.E.M. of PI positive neurons for each treatment showed in **Fig. 4A** and **Fig. S1D**. H_2O_2 treatment (50 µM for 5 hours; **Fig. S1D**) was included as positive control for necrotic cell death (n = 3, one-way ANOVA, ***P<0.001; Tukey's post-test: ***, show significant differences with vehicle treatment). Quantifications were done from three independent cultures, each one with three replicates for each treatment.

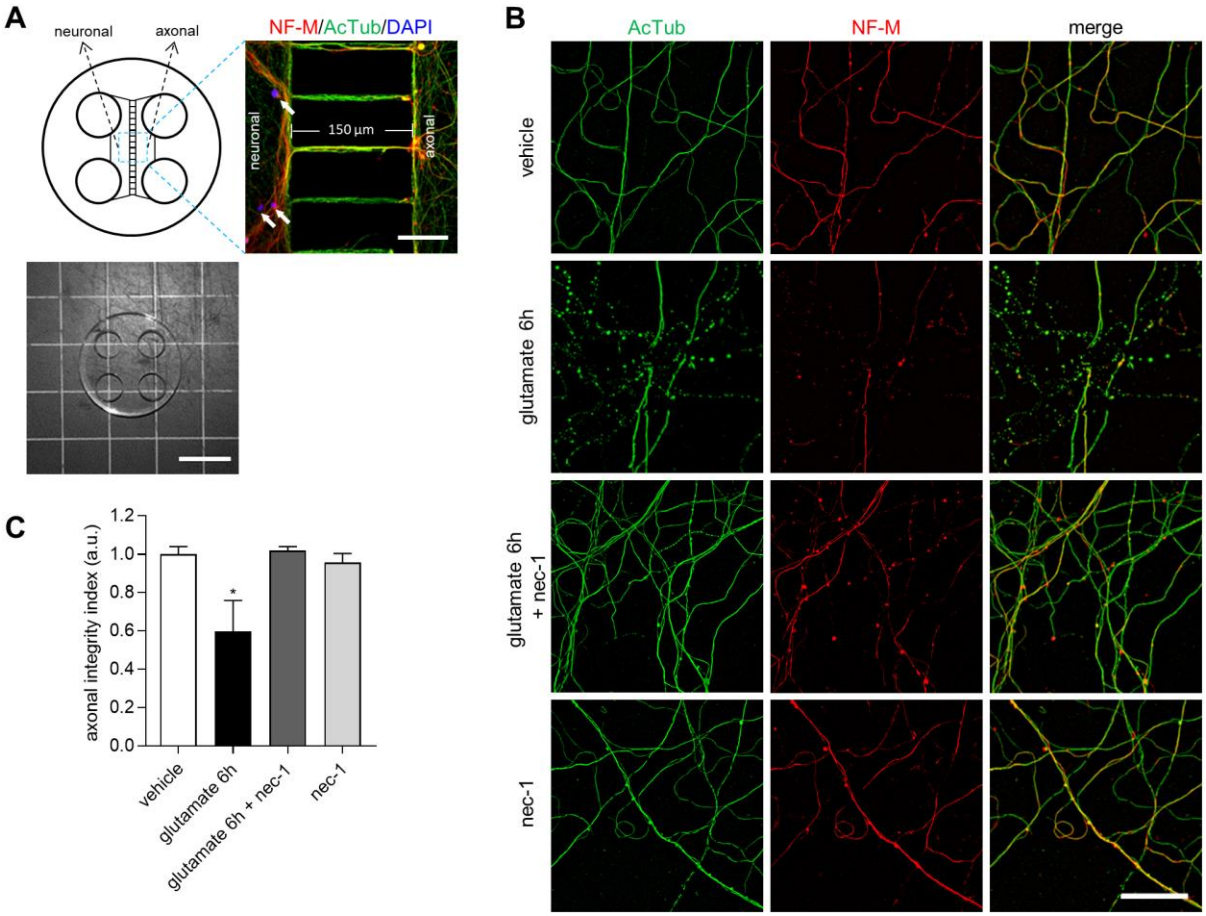

Figure 5. Axonal RIPK1 inhibition delays axonal degeneration compartmentalized hippocampal neuron cultures exposed to glutamate in the neuronal soma. (**A**) **Top left**: Schematic drawing of the microfluidic device showing the neuronal and axonal compartments. **Top right**: microscopy picture showing the detail of the microgroove area and part of the neuronal compartments in a 14-15DIV hippocampal neuron compartmentalized culture. Neurons were immunostained with AcTub (green), NF-M (red) and DAPI as nuclear stain (blue). Arrows depict neuronal soma at the neuronal side of the compartmentalized culture. Axons span across the microgrooves into the axonal compartment. Scale bar, 50 µm. **Bottom left**: Photography of microfluidic device with 150 µm microgrooves. Scale bar, 1 cm. (**B**) Images of the axonal compartment from representative 14-15DIV compartmentalized cultures subjected to vehicle or glutamate (20 µM for 6 hours) treatment in the neuronal compartment with or without nec1 pre-treatment in the axonal compartment (100 µM for 18 hours). Axons were immunostained for AcTub (green), NF-M (red) and DAPI nuclear stain was used to show absence of neuronal soma in the axonal compartment. Scale bar, 50 µm. (**C**) Axonal integrity quantification for all the treatments described in **Fig.5B,** using the axonal integrity index ± S.E.M. (n = 3, one-way ANOVA, *P<0.05; Tukey's post-test: * show significant differences with vehicle treatments). Quantifications were done from three independent compartmentalized cultures for each treatment.

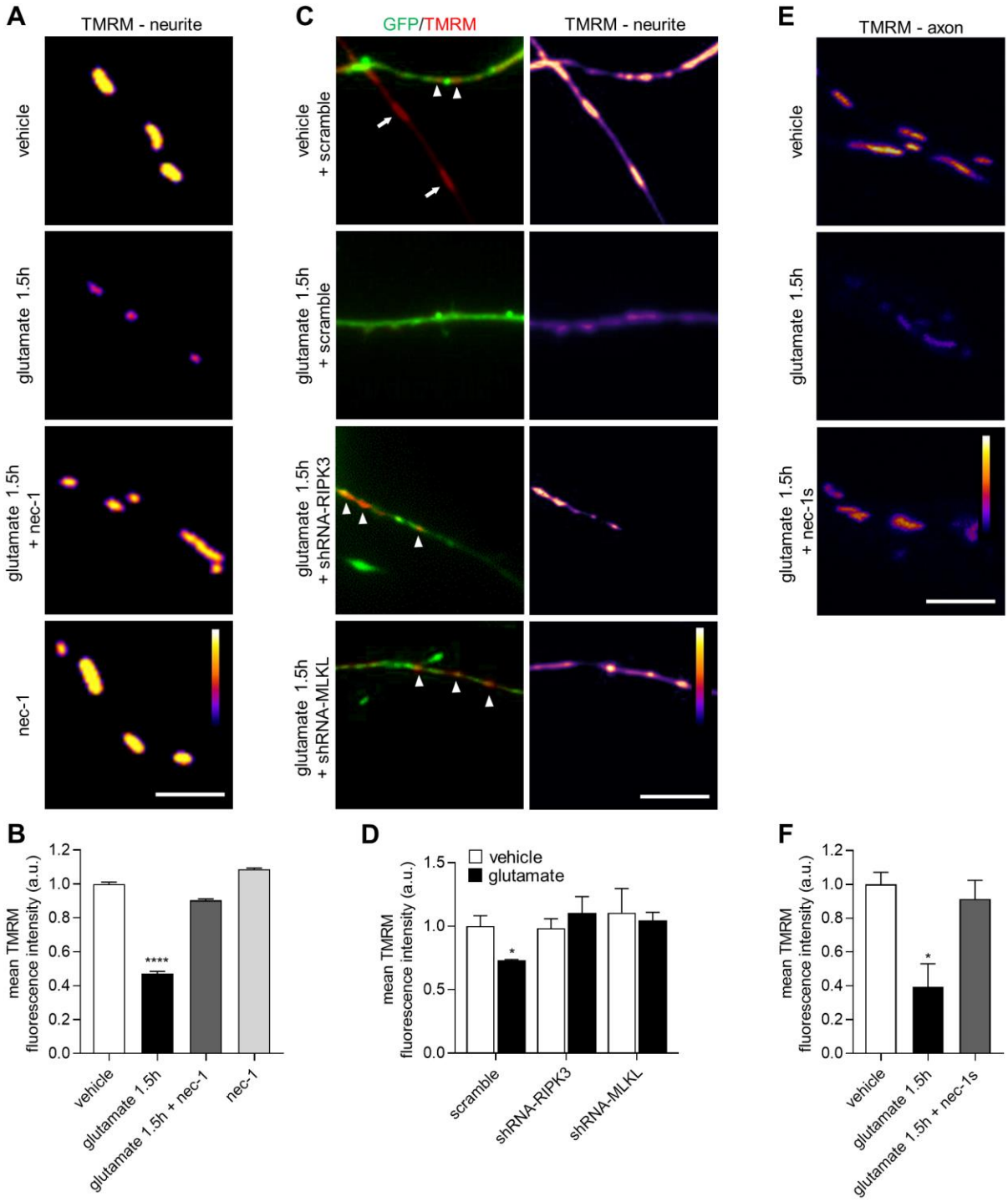

Figure 6. RIPK1, RIPK3 and MLKL inhibition prevents the glutamate induced decrease in mitochondrial potential observed in axonal/neurite mitochondria. (**A**) Live-cell imaging of neurite mitochondrion from dissociated 7-8DIV hippocampal neuronal cultures stained with TMRM, a mitochondrial potential sensitive dye. Cultures were treated with vehicle or glutamate (20 µM for 1.5 hours) with or without nec-

1 pre-treatment (100 µM for 18 hours). Scale bar, 2 µM. (**B**) Mean relative mitochondrial TMRM fluorescence intensity ± S.E.M for all treatments described in **Fig. 6A** (n = 3, Kruskal-Wallis Test, ****P<0.0001; Dunn's post-test: ***, show significant differences with vehicle treatment). (**C**) Neurite mitochondria from dissociated 7-8DIV hippocampal neuronal cultures infected with lentiviruses expressing shRNA against RIPK3, MLKL or a scramble control sequence and treated with vehicle or glutamate (20 µM for 1.5 hours) were stained with TMRM as mitochondrial potential reporter. Viral genetic construct co-express GFP as reporter gene for infected neurons. **Left column**: Fluorescence of GFP (green) and TMRM (red). Arrowheads depict TMRM positive mitochondria in GFP positive neurites. Arrows show TMRM positive mitochondria in GFP negative neurites. **Right column**: TMRM intensity profile images for all the described treatments. Scale bar, 10 µm. Vehicle treated controls of neurons expressing shRNA-RIPK3 and shRNA-MLKL are shown in **Fig. S5B**. (**D**) Mean relative mitochondrial TMRM fluorescence intensity ± S.E.M for all treatments described in panel C (n = 3, Kruskal-Wallis Test, *P<0.05; Dunn's post-test: *, show significant differences with vehicle treatment in scramble shRNA expressing neurons). For non-compartmentalized culture experiments, quantifications were done from three independent cultures, each one with three replicates for each treatment. (**E**) Axonal mitochondria stained with TMRM from 14-15DIV compartmentalized hippocampal neuronal cultures as the ones shown in **Fig. 5A**. Cultures were treated with vehicle or glutamate (20 µM for 1.5 hours) in the neuronal compartment, with or without nec-1s pre-treatment in the axonal compartment (100 µM for 18 hours). Scale bar, 2 µM (**F**) Mean relative mitochondrial TMRM fluorescence intensity ± S.E.M for all treatments described in panel E (n = 3, Kruskal-Wallis Test, *P<0.05; Dunn's post-test: *, show significant differences with vehicle treatment). Color map: relative level of TMRM fluorescence form less (blue) to high (white) fluorescence intensity. For compartmentalized culture experiments, quantifications were done from three independent compartmentalized cultures for each treatment.

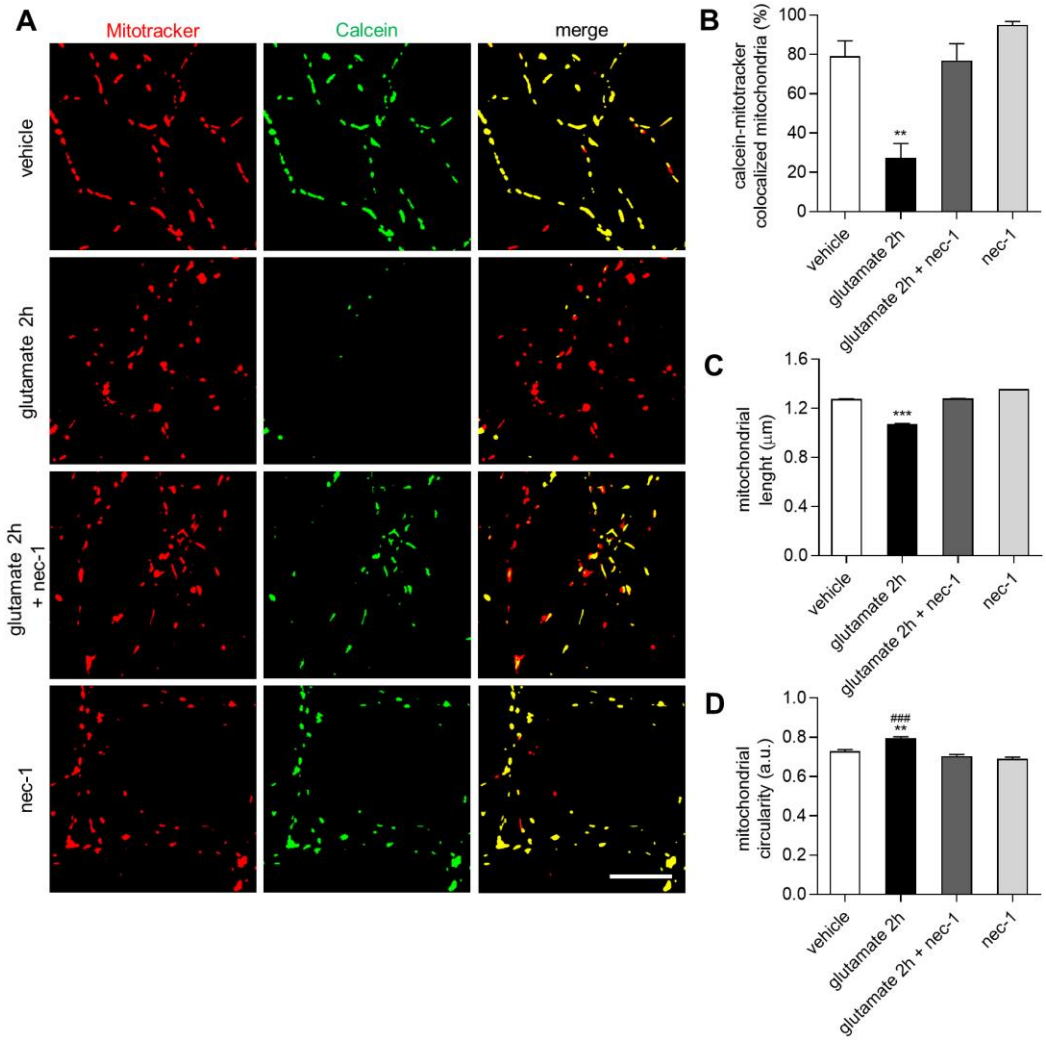

Figure 7. RIPK1 inhibition prevents mPTP opening and morphology changes induced by glutamate treatment in neurite mitochondria. (**A**) Live cell imaging of neurite mitochondrion stained with mitotracker (red; **left**), calcein (green; **center**) and co-localization (yellow; **right**) for the calcein-cobalt mPTP-opening evaluation assay (see methods). Neurons were treated with vehicle or glutamate (20 µM glutamate for 2 hours) with or without nec-1 pre-treatment (100 µM for 18 hours). Scale bar, 10 µm. (**B**) Percentage of co-localization ± S.E.M. between mitotracker and calcein mitochondrial stains for all the treatments described in panel A (n = 3, one-way ANOVA, **P<0.01; Tukey's post-test: **, show significant differences with vehicle treatment other treatment). Morphology analysis was performed in neurites using mitotracker mitochondrial stain from images as the ones shown in panel A (left column)**.** Mean mitochondrial length ± S.E.M (**B**) and mean mitochondrial circularity ± S.E.M. (**C**), from neurons exposed to vehicle or glutamate (20 µM for 2 hours) treatments, with or without nec-1 pre-treatment (100 µM for 18 hours) (n = 3, one-way ANOVA, ** *P*<0.01, *** *P*<0.001; Tukey's post-test: *'s, show significant differences with vehicle treatment). Quantifications were done from three independent cultures, each one with three replicates for each treatment.

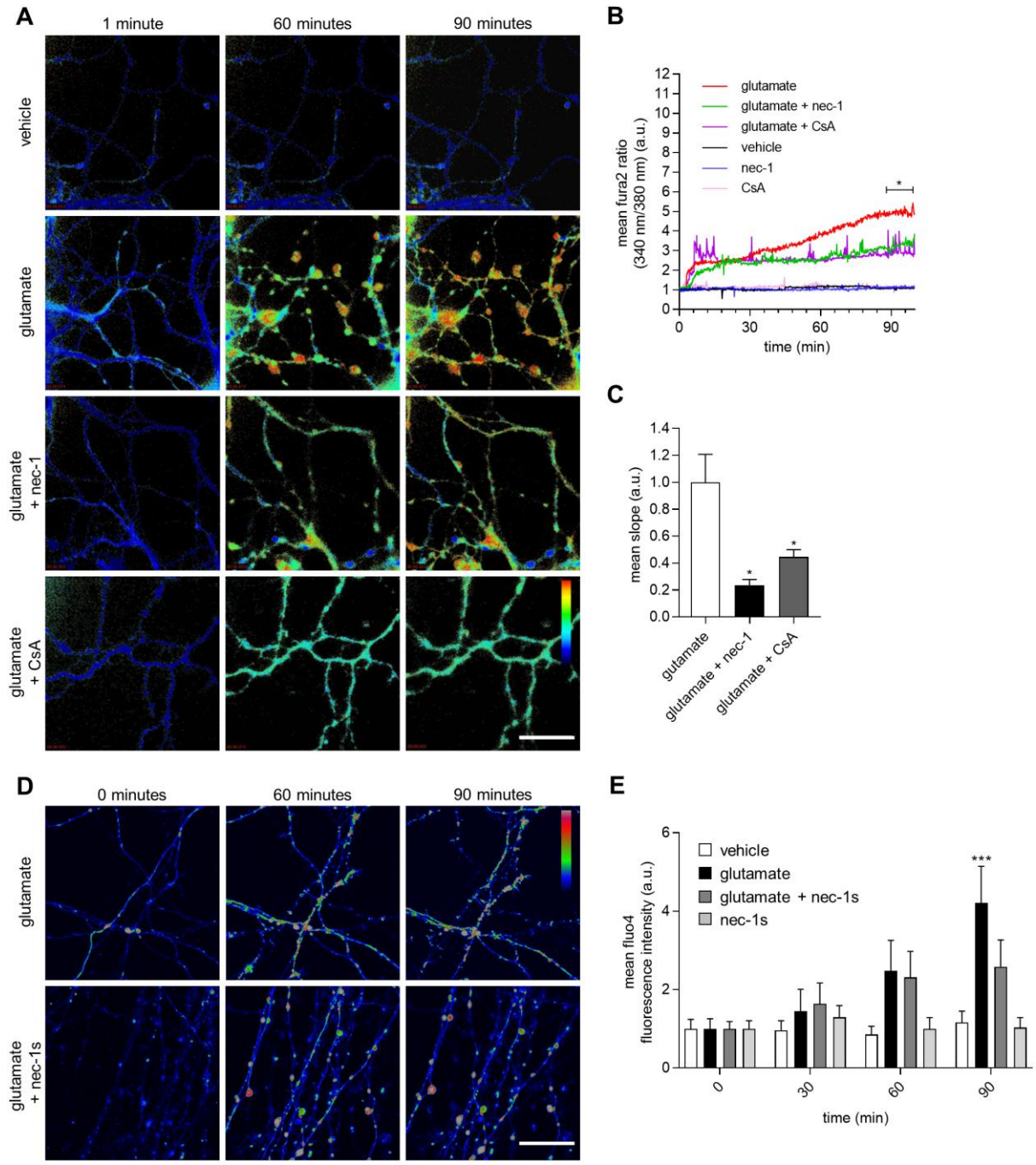

Figure 8 RIPK1 inhibition prevents neurite and axonal calcium dys-homeostasis induced by glutamate treatment in hippocampal neurons exposed to glutamate. (**A**) Representative images of neurite fields from fura-2 (free cytoplasmic Ca^{2+} probe) stained neurites from a live-cell time-lapse experiment. Images at 1 (**left column**), 60 (**center column**) and 90 minutes (**right column**) of recordings are shown. Neuronal cultures were treated with vehicle or glutamate (20 μM at 3 minutes of recording) with

or without nec-1 (100 µM for ~18 hours before the start of time-lapse recording) or CsA (50 µM for 15 minutes before the start of time-lapse recording) pre-treatments. Color bar, ratiometric fluorescence intensity of fura-2 from less (blue) to higher (red) levels. Scale bar, 20 µm. (**B**) Mean traces of ratiometric fura-2 fluorescence intensity levels, from time-lapse recordings obtained from all the treatments described in panel A and including CsA and nec-1 control treatments (n = 3, two-way ANOVA, *P<0.05; Bonferroni's post-test: *, show significant differences with glutamate treatment). (**C**) Mean slopes for glutamate, glutamate + nec-1 and glutamate + CsA treatments, between 30 and 90 minutes of the time-lapse recordings (n = 3, one-way ANOVA, * P<0.05; Tukey's post-test: *, show significant differences with glutamate treatment). Quantifications were done from three independent cultures, each one with three replicates for each treatment. (**D**) Representative images of compartmentalized cultures loaded with Fluo4 in the axonal compartment treated with vehicle or glutamate (20 µM) in the neuronal compartment with or without nec-1s pre-treatment in the axonal compartment (100 µM for 18 hours). Live-cell snapshots of each axonal field in the axonal compartment were recorded before glutamate treatment (0 minutes) and after 60 and 90 minutes of glutamate treatment. Images from control experiments are shown in **Fig. S6C**. Color bar, fluorescence intensity profile of fluo3 from less (blue) to high (brown) levels. Scale bar, 50 µm. (**E**) Mean fluo4 fluorescence intensity ± S.E.M. for each treatment at different snap-shot times. Normalization and statistics for each treatment was done using their corresponding mean '0 minute' basal fluorescence as a reference. (n = 3, one-way ANOVA, *** P<0.001; Tukey's post-test: *, show significant differences with their respective 'minute 0' reference mean fluorescence value). For compartmentalized culture experiments, quantifications were done from three independent compartmentalized cultures for each treatment.

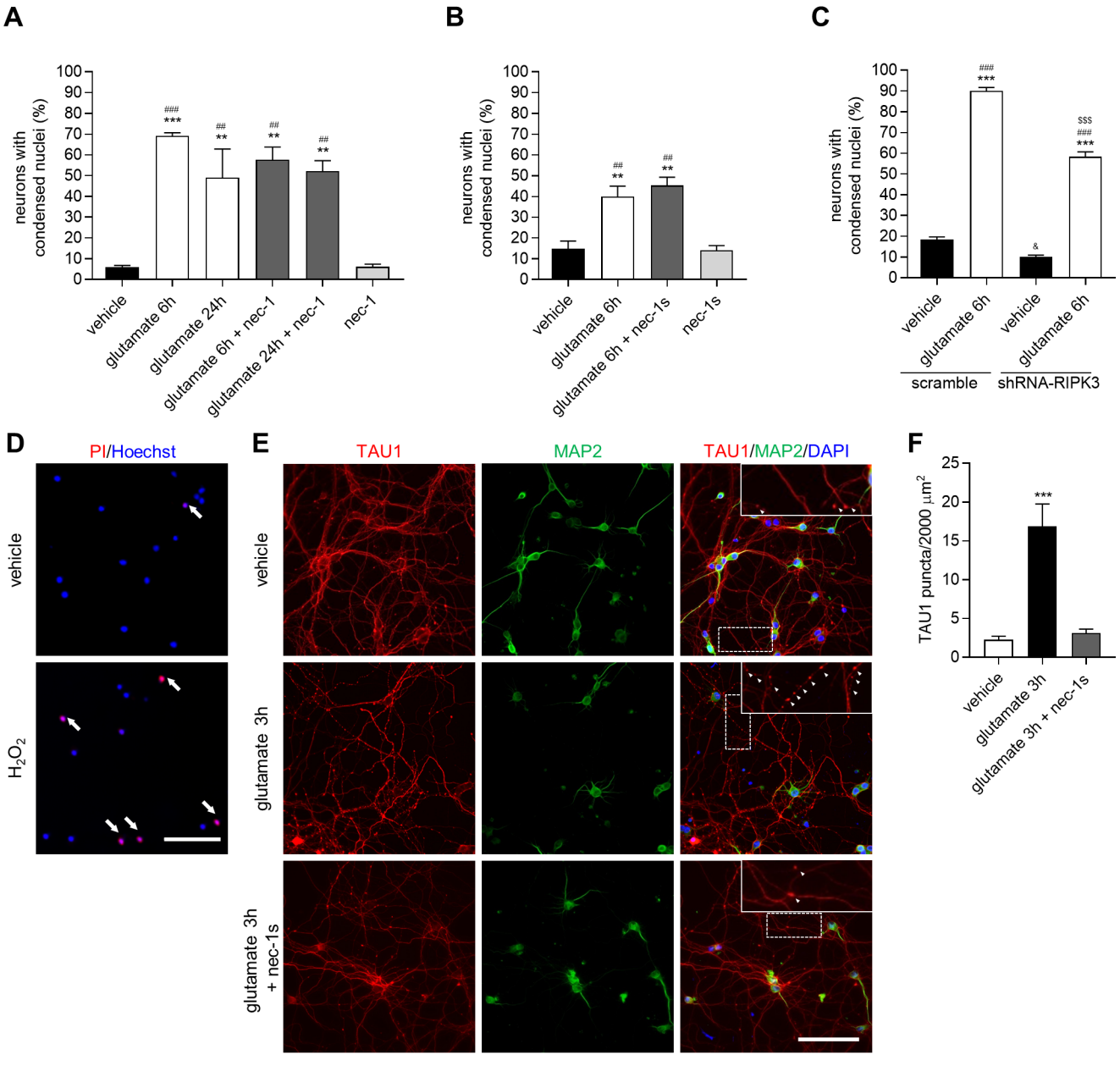

Supplementary Figure 1. (**A**) Mean percentage ± S.E.M. of neurons showing condensed DAPI stain in nec-1 experiments described in **Fig. 1A and Fig. S3A** (n = 3, one-way ANOVA, $^{\#\#}$ and ** P<0.01, $^{\#\#\#}$ and *** P<0.001; Tukey's post-test: *'s show significant differences with vehicle treatment; $^{\#}$'s show significant difference with nec-1 control treatment). (**B**) Mean percentage ± S.E.M. of neurons showing condensed DAPI stain in nec-1s experiments described in **Fig. 1A** (n = 3, one-way ANOVA, $^{\#\#}$ and ** P<0.01; Tukey's post-test: ** show significant differences with vehicle treatment; $^{\#\#}$ show significant difference with nec-1s control treatment). (**C**) Mean percentage ± S.E.M. of neurons showing condensed DAPI stain in experiments described in **Fig. 1B** (n = 3, one-way ANOVA, $^{\&}$ P<0.05, **, $^{\#\#\#}$ and $^{\$\$\$}$ P<0.001; Tukey's post-test: *'s show significant differences with vehicle treatment with scramble shRNA; $^{\#}$'s show significant differences with vehicle RIPK3-shRNA; $^{\$}$'s show significant differences between glutamate shRNA scramble and shRNA-RIPK3 treatments; $^{\&}$'s show significant differences between vehicle shRNA-scramble and vehicle shRNA-RIPK3 treatments. Quantifications were done from three independent cultures, each one with three replicates for each treatment. (**D**) Representative images of vehicle and H_2O_2 (50 μM for 5 hours) treated neurons for PI-exclusion assay experiment described in **Fig. 4A,C.** Arrows depict PI positive nuclei. Scale bar, 100 μm. (**E**) Representative immunofluorescence images of the effect of glutamate treatment over TAU1 (red; axonal) and MAP2 (green; dendritic) immunostainings together with DAPI for nuclear staining. 7-8DIV cultured hippocampal neurons were treated with vehicle or glutamate (20 μM for 3 hours) with or without RIPK1 inhibition (nec-1s; 100 μM for 18h). Insets show detailed images of axons. Arrowheads point puncta structures along the axons. Scale bar, 100 μm. (**F**) Mean number of puncta/2000 μm^2 ± S.E.M. of axons from experiment described in panel E (n=3; one-way ANOVA, *** P<0.001; Tukey's post-test: *** show significant differences with vehicle treatment). Quantifications were done from three independent cultures, each one with three replicates for each treatment.

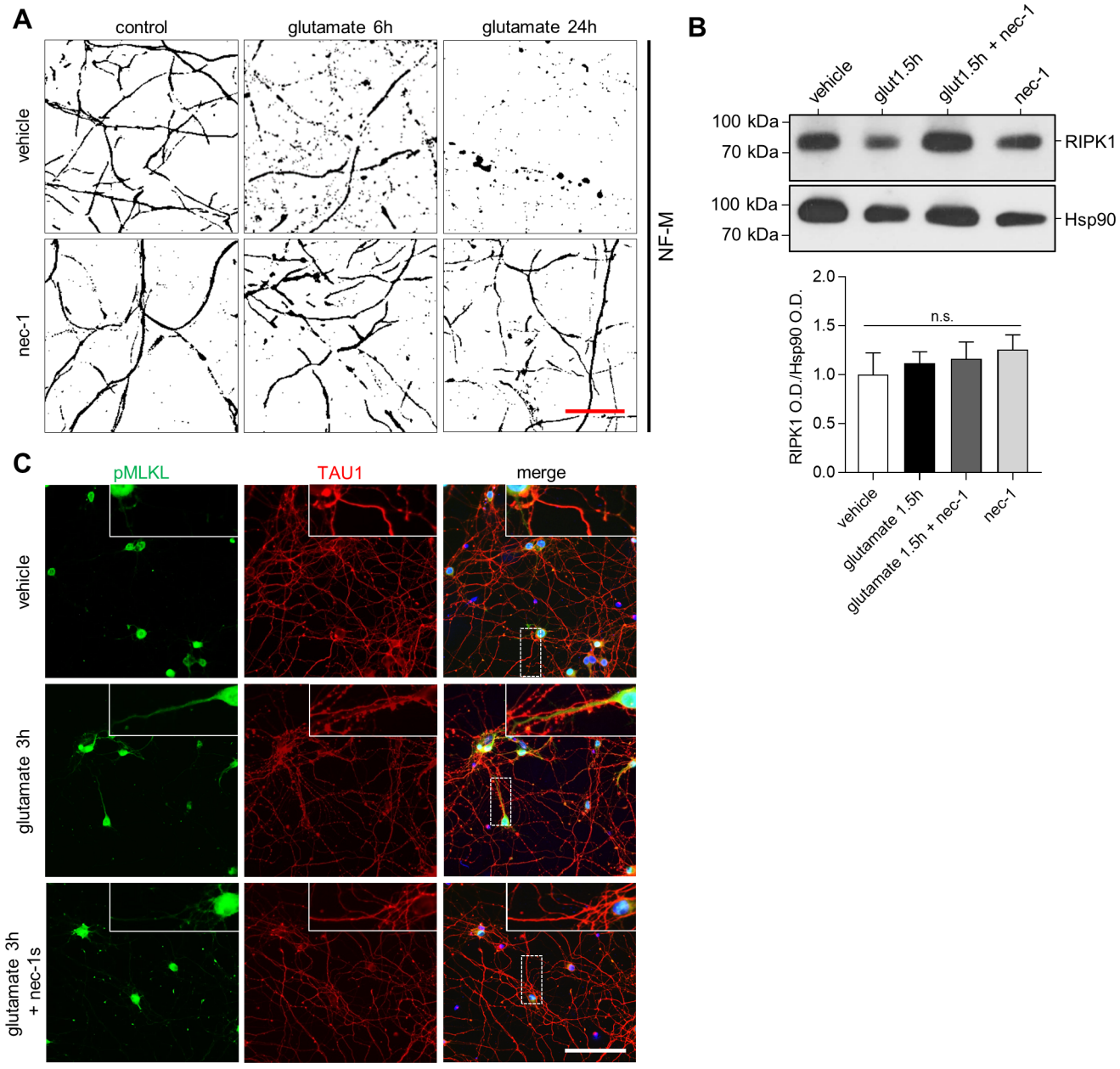

Supplementary Figure 2. (**A**) Binary images of neurites used for neurite degeneration index quantification. Binary images were obtained from primary 7-8DIV hippocampal neuron cultures, exposed to vehicle or glutamate treatment (20 µM for 6 or 24 hours) with or without nec-1 pre-treatment (100 µM for 18 hours), stained for NF-M and binarized (see methods) using imageJ to calculate the neurite integrity index. Scale bar, 20 µm. (**B**) **Top**: RIPK1 western-blot from protein lysates of seven 7-8DIV hippocampal neuronal cultures treated as described in **Fig. 1C**. Hsp90 western-blot was used as loading control. **Bottom**: Densitometric analysis of the relative amount of RIPK1 normalized by Hsp90 ± S.E.M (n = 3, one-way ANOVA, n.s.: non-significant differences). Quantifications were done from three independent cultures, each one with three replicates for each treatment. (**C**) Full images of experiment detailed in **Fig. 1D**. Rectangles show the areas used for the top inset in each image and the images shown in **Fig. 1D**. Scale bar, 100 µm.

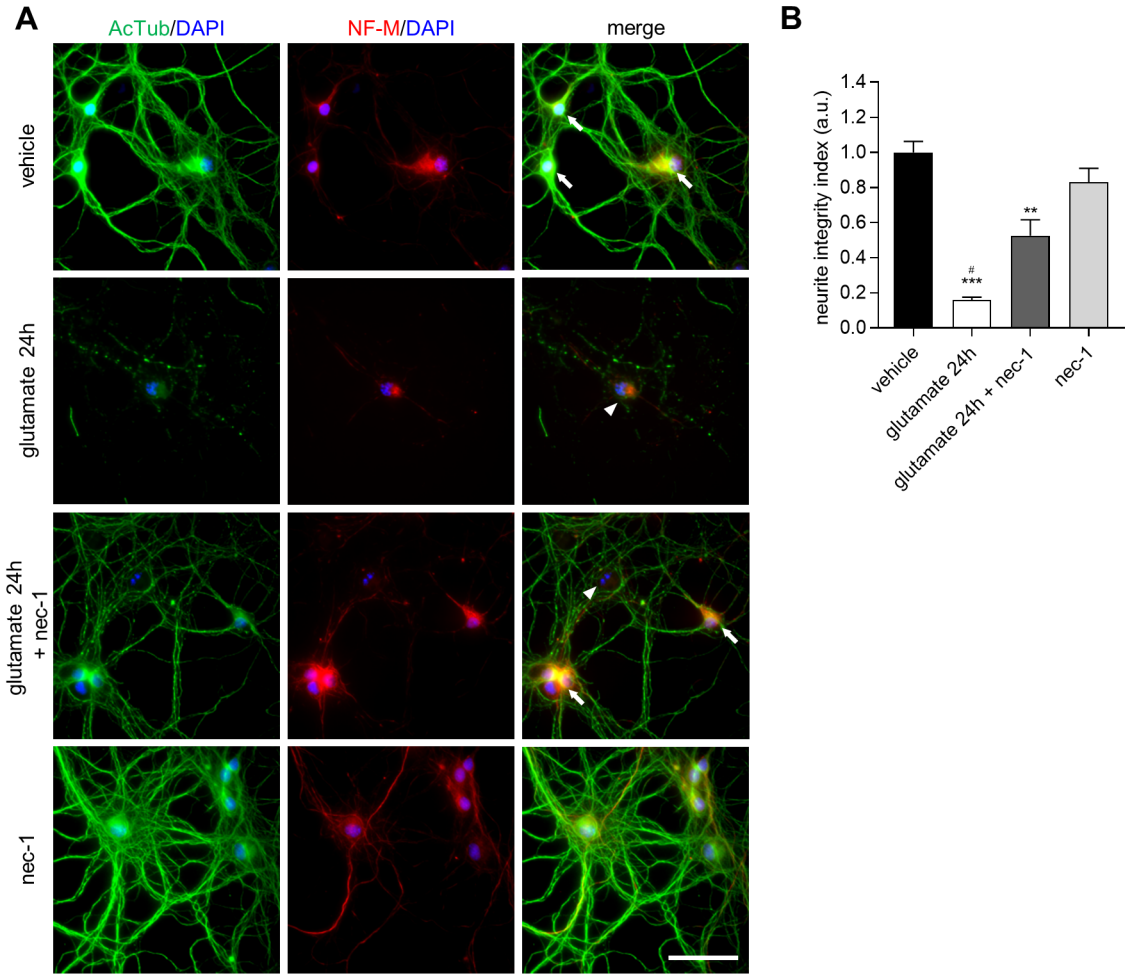

Supplementary Figure 3. (**A**) Dissociated cultured hippocampal neurons immunostained for acetylated tubulin (Ac-Tub, green), neurofilament medium polypeptide (NF-M, red) and DAPI nuclear staining (blue). Cultures were treated with vehicle or glutamate (20 µM for 24 hours) with or without nec-1 pre-treatment (100 µM for 18 hours). Arrows and arrowheads indicate healthy and condensed neuronal somas, respectively. Scale bar, 50 µm. (**B**) Neurite integrity quantification from immunostained neurons as in panel A, evaluated with the mean neurite integrity index ± S.E.M. (n = 3, one-way ANOVA, $^{\#}P<0.05$, $^{**}P<0.01$, $^{***}P<0.001$; Tukey's post-test: *'s show significant differences with vehicle treatment; $^{\#}$'s show significant differences with nec-1 control treatments).

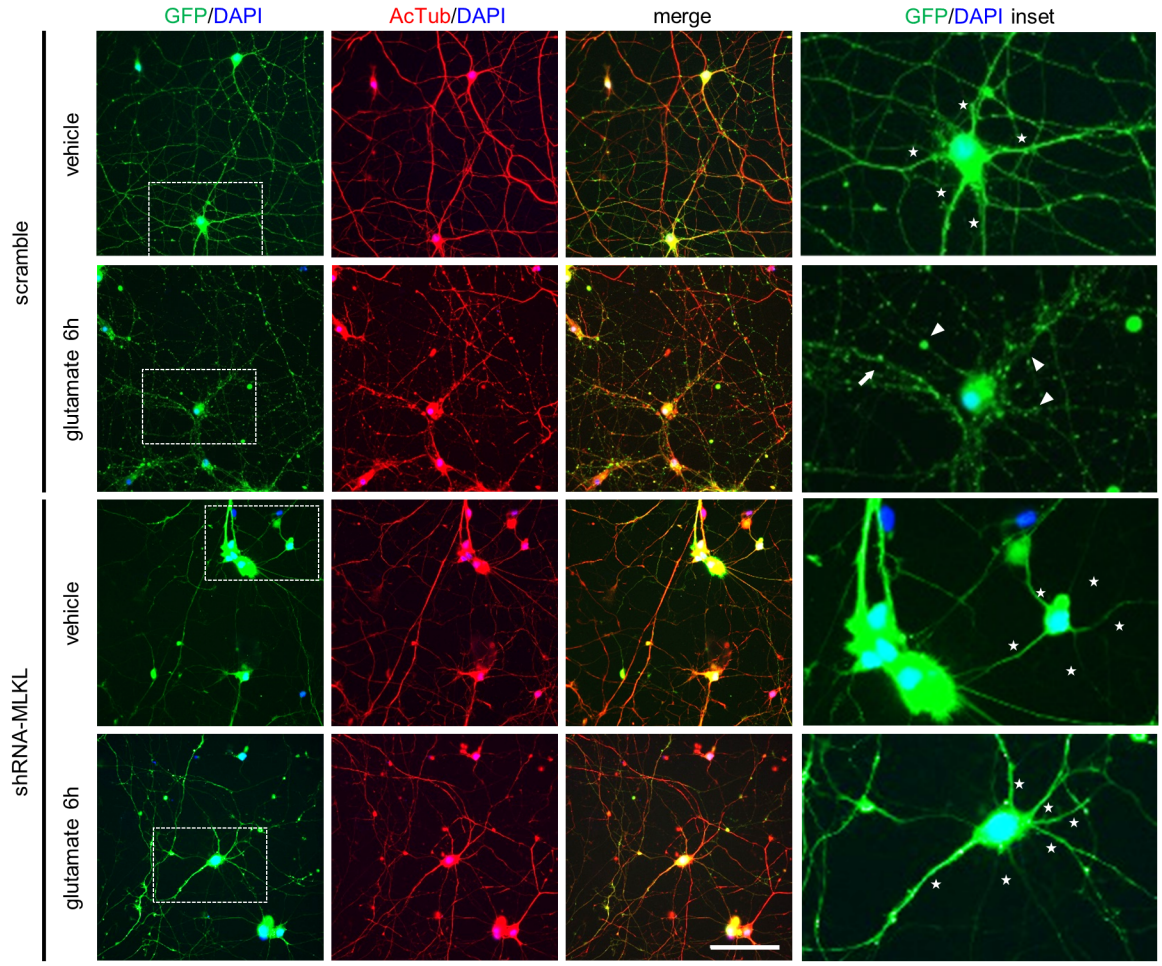

Supplementary Figure 4. Representative images of experiment quantified in **Fig. 3E**. 7-8DIV cultured hippocampal neurons were infected with lentivirus that express shRNA to knock-down MLKL (shRNA-MLKL) or a scramble sequence (scramble) and co-express GFP as reporter gene. Cultures were exposed to vehicle or glutamate (20 μM for 6 hours), fixed and immunostained against GFP (green) and AcTub (red) and stained with DAPI for nuclei visualization. Rectangles in first column detail the origin of the insets shown in the 4th column. Stars depict the presence of neurites with a continuous morphology, arrows show beaded neurites and arrowheads fragmented neurites. Scale bar, 50 μm.

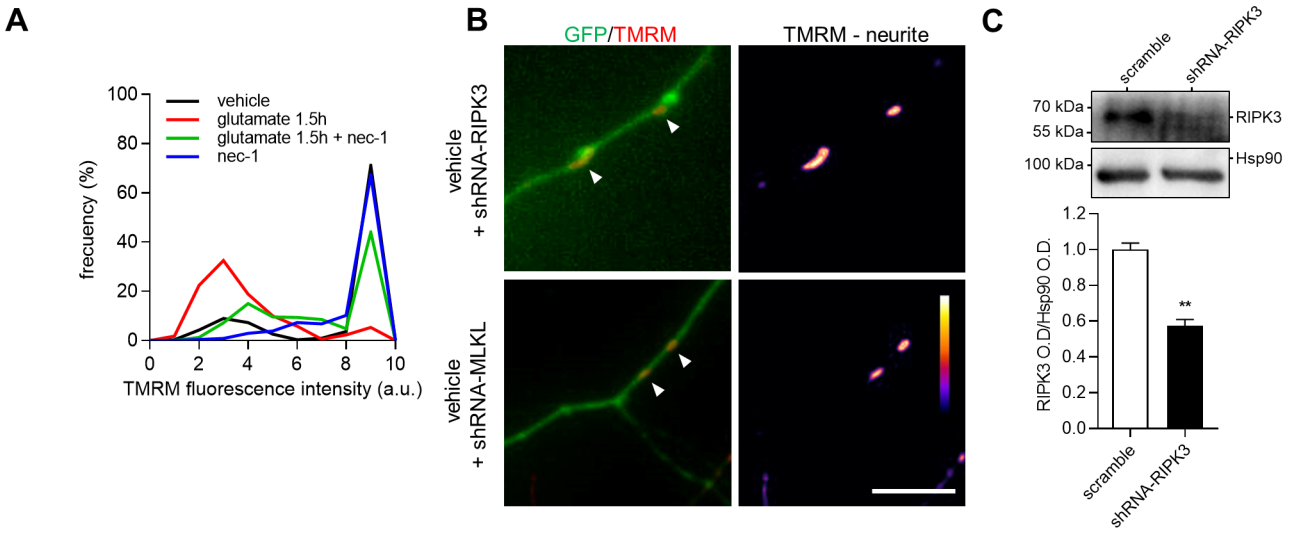

Supplementary Figure 5. (**A**) Frequency distribution histogram of mitochondrial TMRM fluorescence relative intensity for all the treatments described in **Fig. 6A**. Bimodal distribution for al treatments are consistent with significant Shapiro-Wilk normality Test (P<0.001), that show TMRM data distribution for all treatments is non-parametric. (**B**) Representative images of shRNA-RIPK3 and shRNA-MLKL vehicle treatment controls of experiment explained in **Fig. 6C,D. Left column**: Fluorescence of GFP (green) and TMRM (red). Arrowheads depict TMRM positive mitochondria in GFP positive neurites. Arrowheads show TMRM positive mitochondria in GFP positive neurites. **Right column**: TMRM intensity profile images for all the described treatments. Color map: relative level of TMRM fluorescence form less (blue) to high (white) fluorescence intensity. Scale bar, 10 μm. (**C**) **Top**: Western-blot of RIPK3 from 7-8 DIV protein lysates of hippocampal neuron cultures, infected with lentivirus that express scramble shRNA or RIPK3-shRNA. Hsp90 western-blot was used as loading control. **Bottom**: Densitometric analysis of the relative RIPK3 levels normalized by Hsp90 ± S.E.M (n = 3, unpaired, two-tailed, t-Test, **P<0.01). Quantifications were done from three independent cultures, each one with three replicates for each treatment.

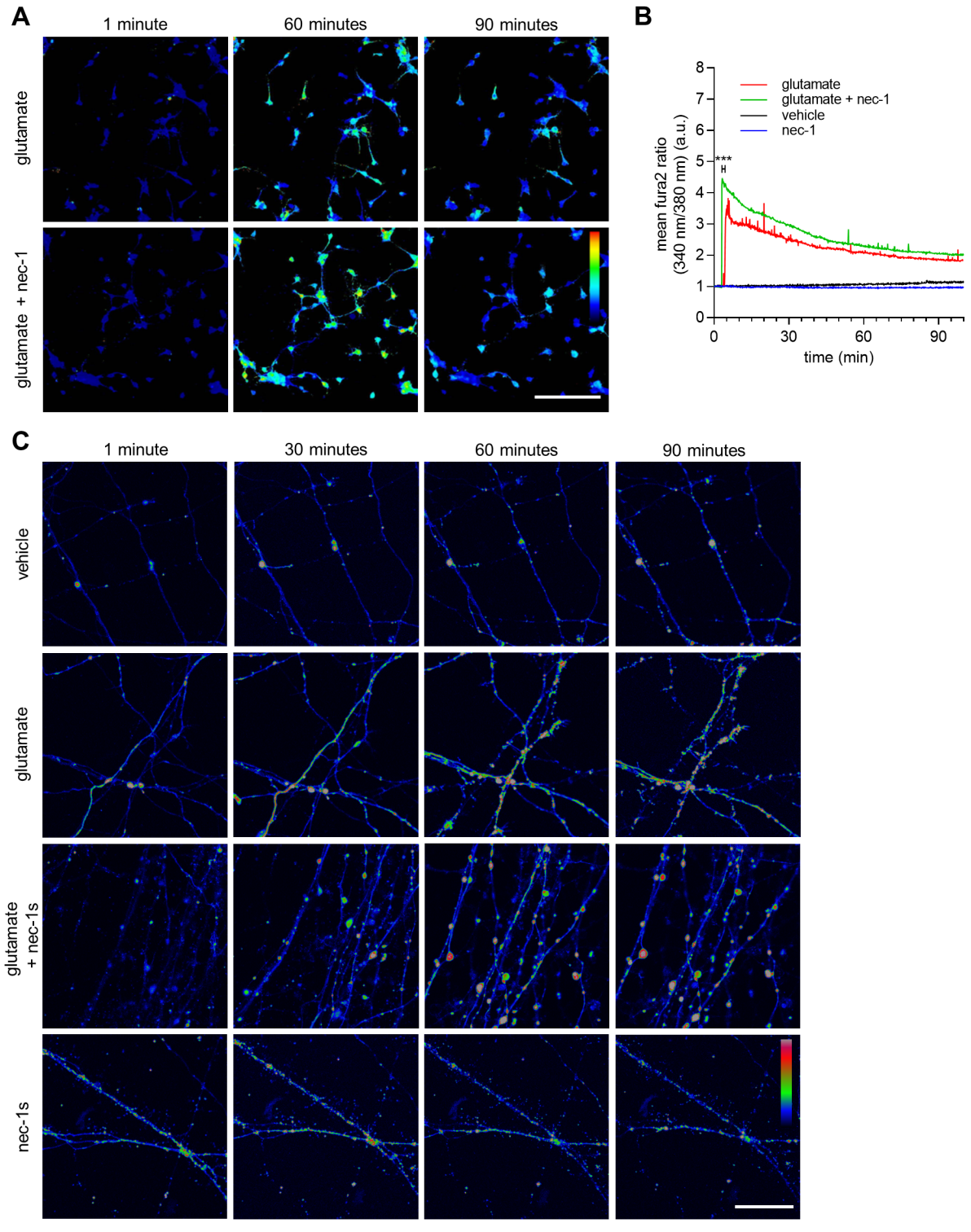

Supplementary Figure 6. (**A**) Calcium dynamics in neuronal soma obtained from time-lapse recordings using the same treatment protocol as in **Fig. 8A.** Time-lapse representative images of neuronal soma stained with Fura-2 cytoplasmic Ca^{2+} sensitive dye, at 1, 60 and 90 minutes of recording. Neuronal cultures were treated with vehicle or glutamate (20 μM at 3 minutes of recording) with or without nec-1 pre-treatment (100 μM for ~18 hours before the start of time-lapse recording). Color bar: Ratiometric fluorescence intensity of fura-2 from less (blue) to higher (red) levels. Scale bar, 100 μm. (**B**) Mean ratiometric fura-2 fluorescence intensity levels, from time-lapse recording obtained from the different treatments indicated in **Fig. S6A** (n = 3, two-way ANOVA, ***P<0.001; Bonferroni's post-test: *'s, show significant differences between vehicle and other treatments). (**C**) Complete panel with representative images from experiment described in **Fig. 8C,D**. Color bar, fluorescence intensity profile of fluo3 from less (blue) to high (brown) levels. Scale bar, 50 μm.

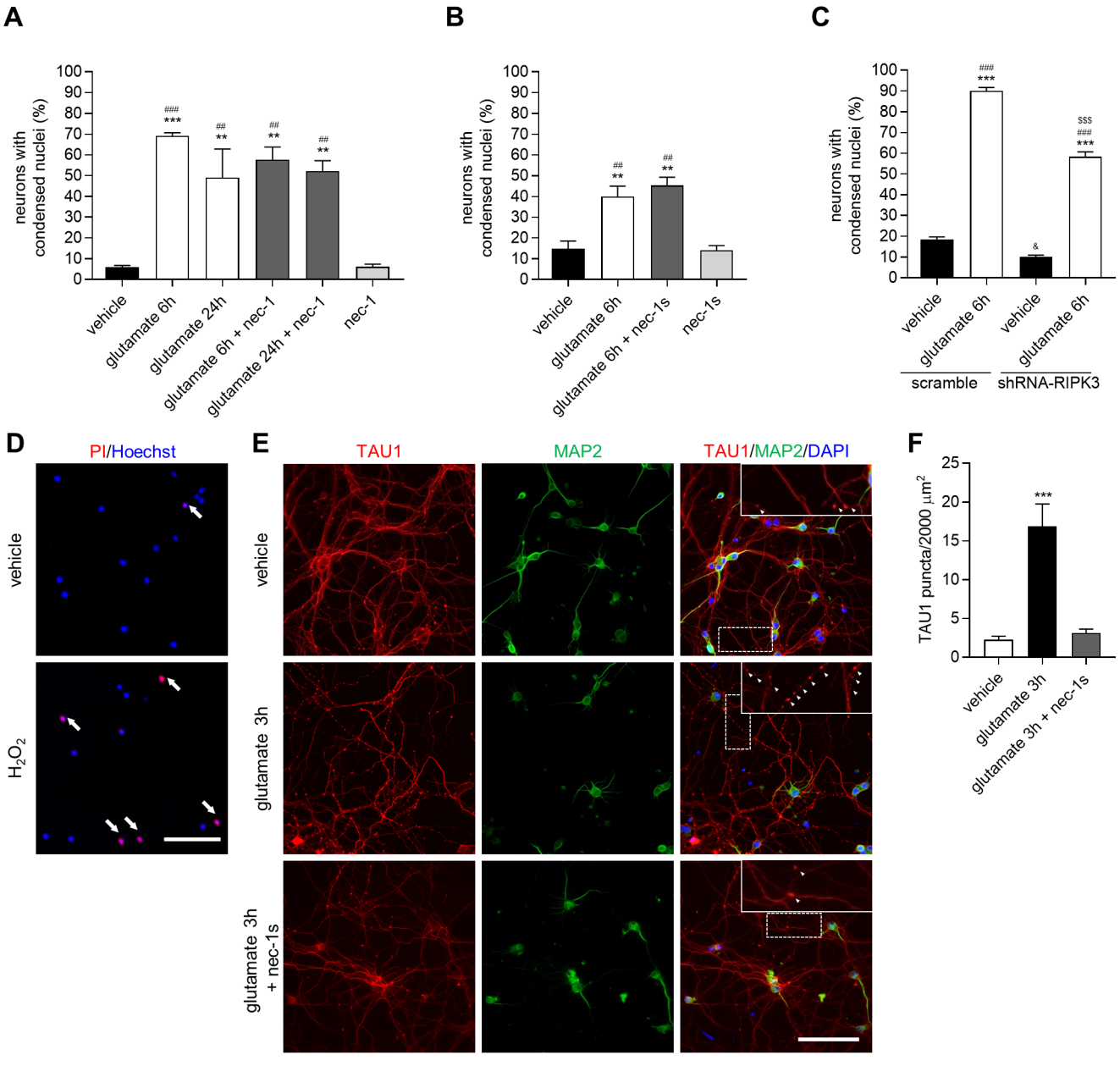

Supplementary Figure 1. (**A**) Mean percentage ± S.E.M. of neurons showing condensed DAPI stain in nec-1 experiments described in **Fig. 1A and Fig. S3A** (n = 3, one-way ANOVA, $^{\#\#}$ and ** P<0.01, $^{\#\#\#}$ and *** P<0.001; Tukey's post-test: *'s show significant differences with vehicle treatment; $^{\#}$'s show significant difference with nec-1 control treatment). (**B**) Mean percentage ± S.E.M. of neurons showing condensed DAPI stain in nec-1s experiments described in **Fig. 1A** (n = 3, one-way ANOVA, $^{\#\#}$ and ** P<0.01; Tukey's post-test: ** show significant differences with vehicle treatment; $^{\#\#}$ show significant difference with nec-1s control treatment). (**C**) Mean percentage ± S.E.M. of neurons showing condensed DAPI stain in experiments described in **Fig. 1B** (n = 3, one-way ANOVA, $^{\&}$ P<0.05, **, $^{\#\#\#}$ and $^{\$\$\$}$ P<0.001; Tukey's post-test: *'s show significant differences with vehicle treatment with scramble shRNA; $^{\#}$'s show significant differences with vehicle RIPK3-shRNA; $^{\$}$'s show significant differences between glutamate shRNA scramble and shRNA-RIPK3 treatments; $^{\&}$'s show significant differences between vehicle shRNA-scramble and vehicle shRNA-RIPK3 treatments. Quantifications were done from three independent cultures, each one with three replicates for each treatment. (**D**) Representative images of vehicle and H_2O_2 (50 μM for 5 hours) treated neurons for PI-exclusion assay experiment described in **Fig. 4A,C.** Arrows depict PI positive nuclei. Scale bar, 100 μm. (**E**) Representative immunofluorescence images of the effect of glutamate treatment over TAU1 (red; axonal) and MAP2 (green; dendritic) immunostainings together with DAPI for nuclear staining. 7-8DIV cultured hippocampal neurons were treated with vehicle or glutamate (20 μM for 3 hours) with or without RIPK1 inhibition (nec-1s; 100 μM for 18h). Insets show detailed images of axons. Arrowheads point puncta structures along the axons. Scale bar, 100 μm. (**F**) Mean number of puncta/2000 μm^2 ± S.E.M. of axons from experiment described in panel E (n=3; one-way ANOVA, *** P<0.001; Tukey's post-test: *** show significant differences with vehicle treatment). Quantifications were done from three independent cultures, each one with three replicates for each treatment.

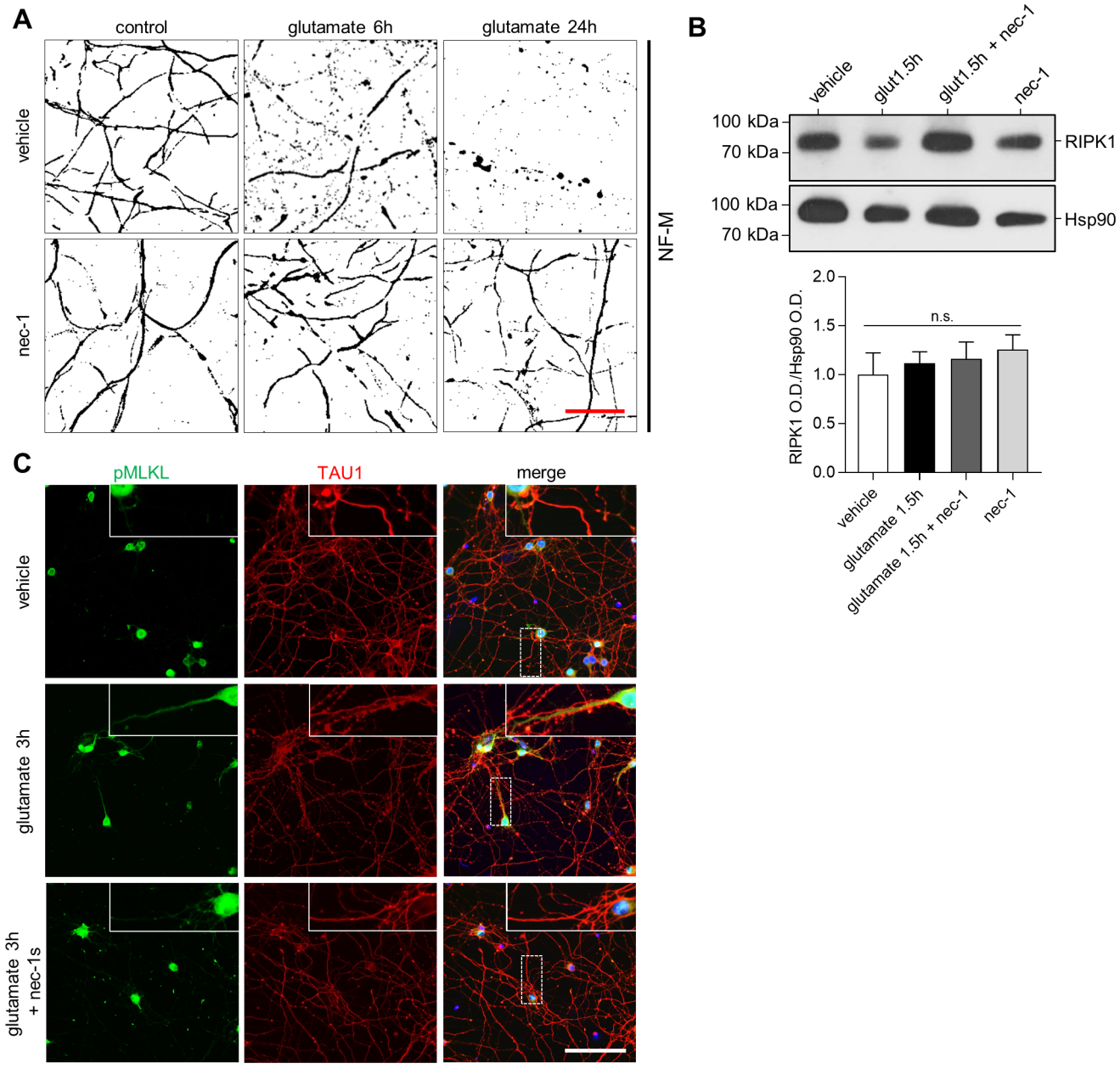

Supplementary Figure 2. (**A**) Binary images of neurites used for neurite degeneration index quantification. Binary images were obtained from primary 7-8DIV hippocampal neuron cultures, exposed to vehicle or glutamate treatment (20 µM for 6 or 24 hours) with or without nec-1 pre-treatment (100 µM for 18 hours), stained for NF-M and binarized (see methods) using imageJ to calculate the neurite integrity index. Scale bar, 20 µm. (**B**) **Top**: RIPK1 western-blot from protein lysates of seven 7-8DIV hippocampal neuronal cultures treated as described in **Fig. 1C**. Hsp90 western-blot was used as loading control. **Bottom**: Densitometric analysis of the relative amount of RIPK1 normalized by Hsp90 ± S.E.M (n = 3, one-way ANOVA, n.s.: non-significant differences). Quantifications were done from three independent cultures, each one with three replicates for each treatment. (**C**) Full images of experiment detailed in **Fig. 1D**. Rectangles show the areas used for the top inset in each image and the images shown in **Fig. 1D**. Scale bar, 100 µm.

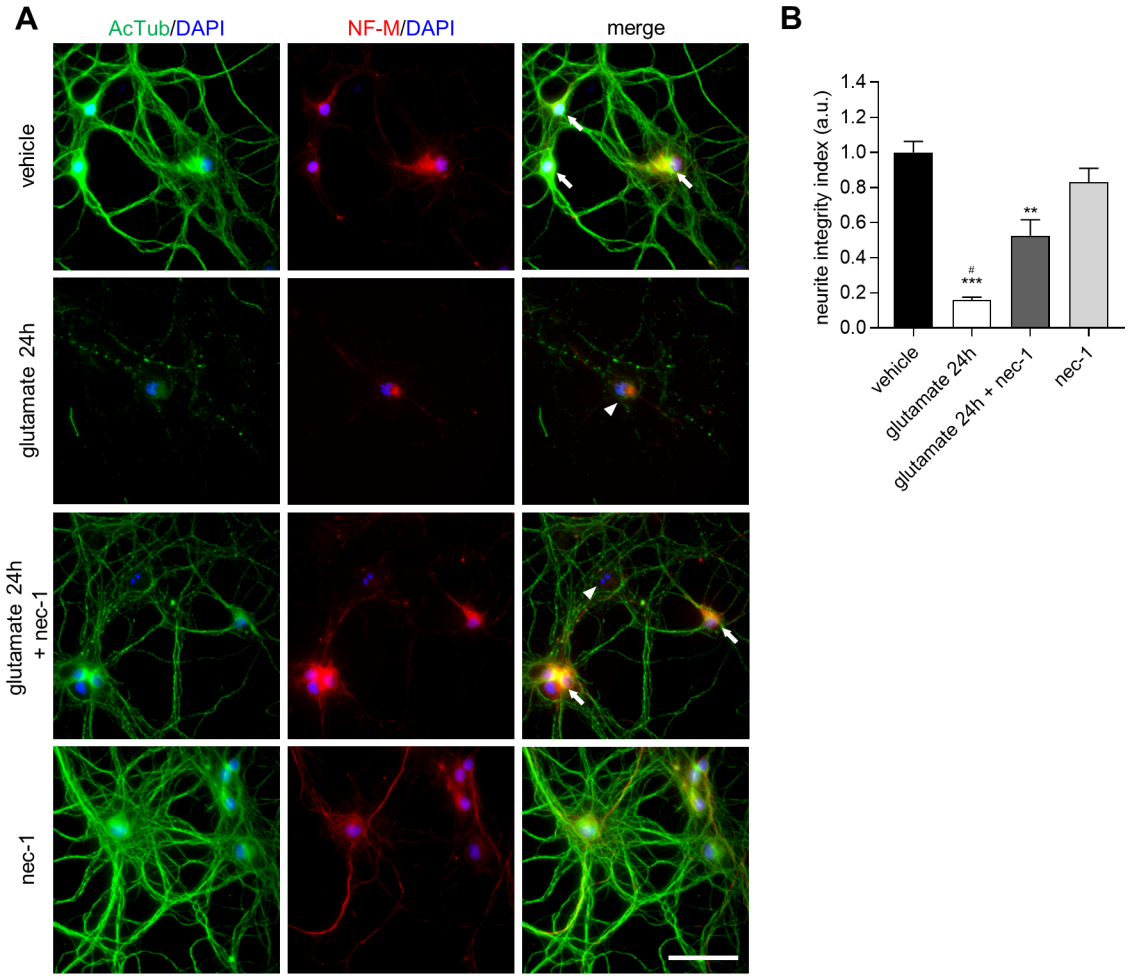

Supplementary Figure 3. (**A**) Dissociated cultured hippocampal neurons immunostained for acetylated tubulin (Ac-Tub, green), neurofilament medium polypeptide (NF-M, red) and DAPI nuclear staining (blue). Cultures were treated with vehicle or glutamate (20 µM for 24 hours) with or without nec-1 pre-treatment (100 µM for 18 hours). Arrows and arrowheads indicate healthy and condensed neuronal somas, respectively. Scale bar, 50 µm. (**B**) Neurite integrity quantification from immunostained neurons as in panel A, evaluated with the mean neurite integrity index ± S.E.M. (n = 3, one-way ANOVA, $^{\#}P<0.05$, $^{**}P<0.01$, $^{***}P<0.001$; Tukey's post-test: *'s show significant differences with vehicle treatment; $^{\#}$'s show significant differences with nec-1 control treatments).

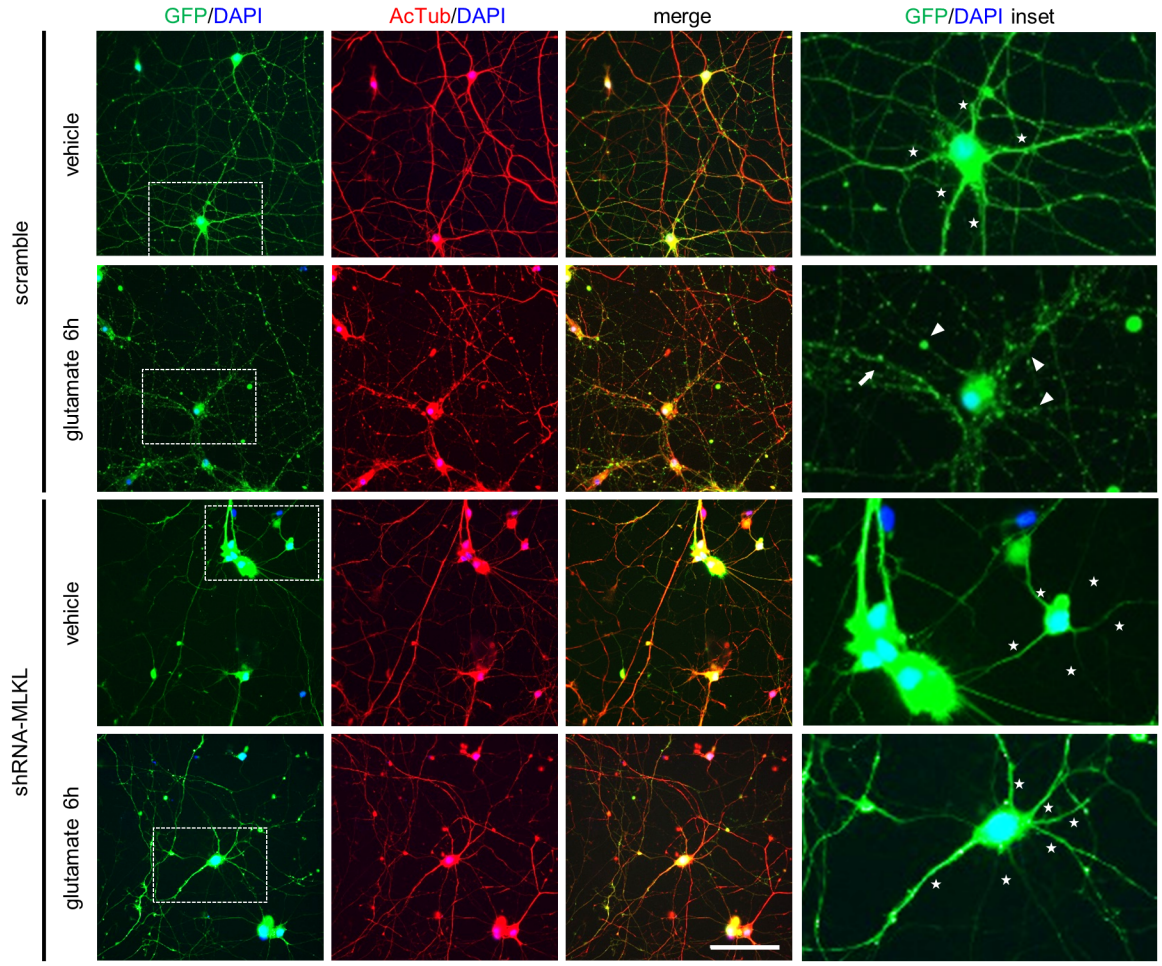

Supplementary Figure 4. Representative images of experiment quantified in **Fig. 3E**. 7-8DIV cultured hippocampal neurons were infected with lentivirus that express shRNA to knock-down MLKL (shRNA-MLKL) or a scramble sequence (scramble) and co-express GFP as reporter gene. Cultures were exposed to vehicle or glutamate (20 μM for 6 hours), fixed and immunostained against GFP (green) and AcTub (red) and stained with DAPI for nuclei visualization. Rectangles in first column detail the origin of the insets shown in the 4th column. Stars depict the presence of neurites with a continuous morphology, arrows show beaded neurites and arrowheads fragmented neurites. Scale bar, 50 μm.

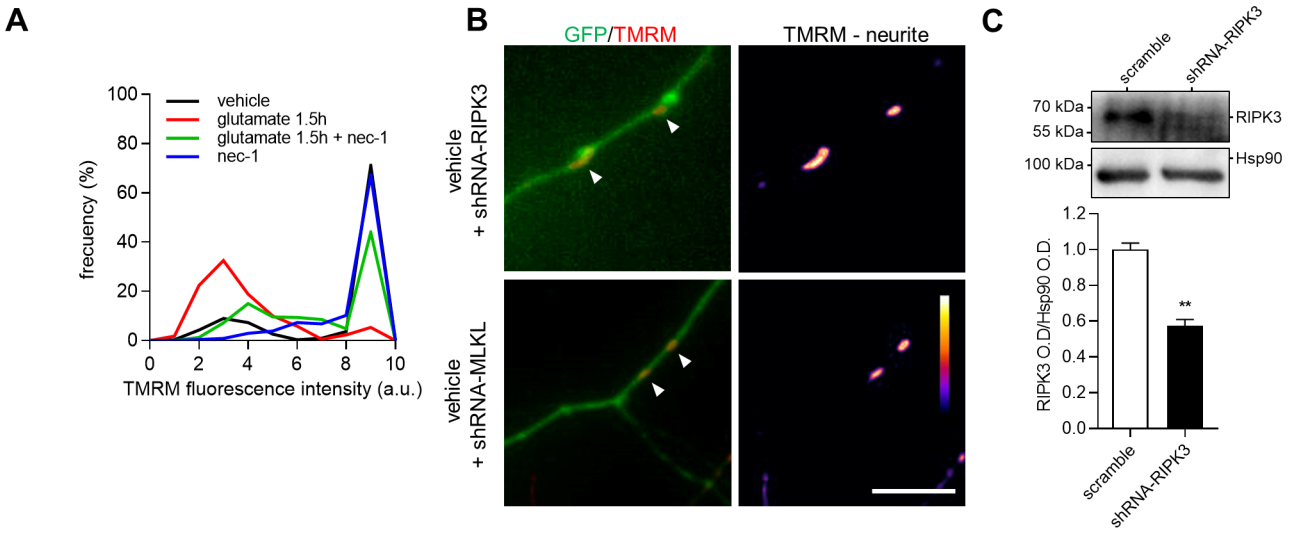

Supplementary Figure 5. (**A**) Frequency distribution histogram of mitochondrial TMRM fluorescence relative intensity for all the treatments described in **Fig. 6A**. Bimodal distribution for al treatments are consistent with significant Shapiro-Wilk normality Test (P<0.001), that show TMRM data distribution for all treatments is non-parametric. (**B**) Representative images of shRNA-RIPK3 and shRNA-MLKL vehicle treatment controls of experiment explained in **Fig. 6C,D. Left column**: Fluorescence of GFP (green) and TMRM (red). Arrowheads depict TMRM positive mitochondria in GFP positive neurites. Arrowheads show TMRM positive mitochondria in GFP positive neurites. **Right column**: TMRM intensity profile images for all the described treatments. Color map: relative level of TMRM fluorescence form less (blue) to high (white) fluorescence intensity. Scale bar, 10 μm. (**C**) **Top**: Western-blot of RIPK3 from 7-8 DIV protein lysates of hippocampal neuron cultures, infected with lentivirus that express scramble shRNA or RIPK3-shRNA. Hsp90 western-blot was used as loading control. **Bottom**: Densitometric analysis of the relative RIPK3 levels normalized by Hsp90 ± S.E.M (n = 3, unpaired, two-tailed, t-Test, **P<0.01). Quantifications were done from three independent cultures, each one with three replicates for each treatment.

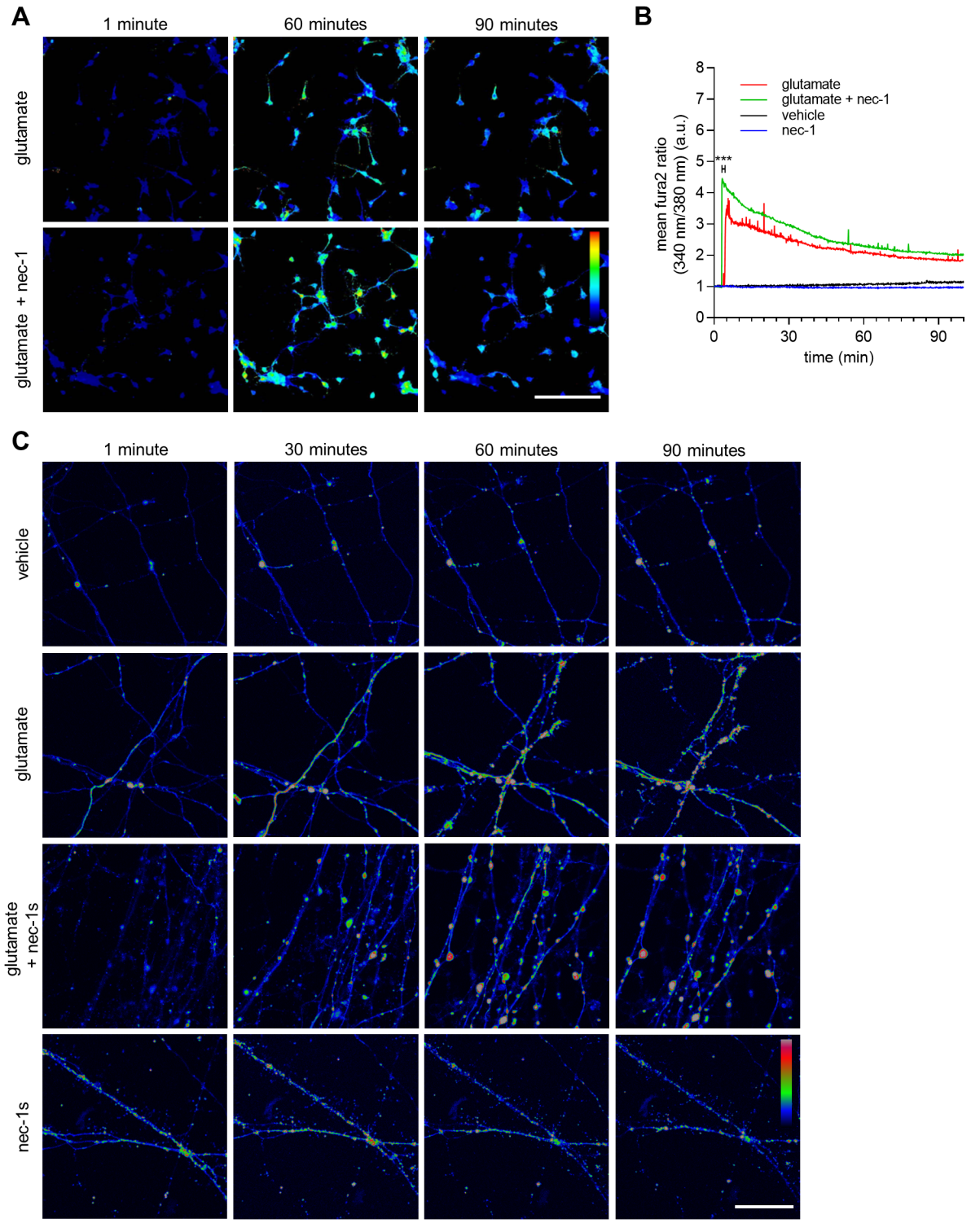

Supplementary Figure 6. (**A**) Calcium dynamics in neuronal soma obtained from time-lapse recordings using the same treatment protocol as in **Fig. 8A.** Time-lapse representative images of neuronal soma stained with Fura-2 cytoplasmic Ca^{2+} sensitive dye, at 1, 60 and 90 minutes of recording. Neuronal cultures were treated with vehicle or glutamate (20 μM at 3 minutes of recording) with or without nec-1 pre-treatment (100 μM for ~18 hours before the start of time-lapse recording). Color bar: Ratiometric fluorescence intensity of fura-2 from less (blue) to higher (red) levels. Scale bar, 100 μm. (**B**) Mean ratiometric fura-2 fluorescence intensity levels, from time-lapse recording obtained from the different treatments indicated in **Fig. S6A** (n = 3, two-way ANOVA, ***P<0.001; Bonferroni's post-test: *'s, show significant differences between vehicle and other treatments). (**C**) Complete panel with representative images from experiment described in **Fig. 8C,D**. Color bar, fluorescence intensity profile of fluo3 from less (blue) to high (brown) levels. Scale bar, 50 μm.